Published online 16 November 2018 *Nucleic Acids Research, 2019, Vol. 47, No. 3* ***1195–1210***
doi: 10.1093/nar/gky1157

Post-mitotic BET-induced reshaping of integrase quaternary structure supports wild-type MLV integration

Doortje Borrenberghs[1,2], Irena Zurnic[2,†], Flore De Wit[2,†], Aline Acke[1,†], Lieve Dirix[1,2], Anna Cereseto[3], Zeger Debyser[2,*] and Jelle Hendrix[1,4,*]

[1]Laboratory for Photochemistry and Spectroscopy, Department of Chemistry, KU Leuven, Celestijnenlaan 200F, B-3001 Leuven, Belgium, [2]Laboratory for Molecular Virology and Gene Therapy, Department of Pharmaceutical and Pharmacological Sciences, KU Leuven, Kapucijnenvoer 33, B-3000 Leuven, Flanders, Belgium, [3]Center for Integrative Biology (CIBIO), University of Trento, I-38123 Trento, Italy and [4]Dynamic Bioimaging Lab, Advanced Optical Microscopy Centre and Biomedical Research Institute (BIOMED), Hasselt University, Agoralaan C, B-3590 Diepenbeek, Belgium

Received February 12, 2018; Revised October 28, 2018; Editorial Decision October 29, 2018; Accepted October 30, 2018

ABSTRACT

The Moloney murine leukemia virus (MLV) is a prototype gammaretrovirus requiring nuclear disassembly before DNA integration. In the nucleus, integration site selection towards promoter/enhancer elements is mediated by the host factor bromo- and extraterminal domain (BET) proteins (bromodomain (Brd) proteins 2, 3 and 4). MLV-based retroviral vectors are used in gene therapy trials. In some trials leukemia occurred through integration of the MLV vector in close proximity to cellular oncogenes. BET-mediated integration is poorly understood and the nature of integrase oligomers heavily debated. Here, we created wild-type infectious MLV vectors natively incorporating fluorescent labeled IN and performed single-molecule intensity and Förster resonance energy transfer experiments. The nuclear localization of the MLV pre-integration complex neither altered the IN content, nor its quaternary structure. Instead, BET-mediated interaction of the MLV intasome with chromatin in the post-mitotic nucleus reshaped its quaternary structure.

INTRODUCTION

Retroviral genera evolved different solutions for infecting resting or dividing cells. Lentiviruses, such as the human immunodeficiency virus type 1 (HIV-1), are capable of infecting non-dividing cells by active transport through the nuclear pore, while gammaretroviruses such as the MLV, gain access to the host chromatin upon nuclear breakdown during mitosis (1–3). After cell entry, the reversely transcribed vDNA forms a large nucleoprotein complex together with the viral integrase enzyme (IN) and other viral and cellular proteins, referred to as the pre-integration complex (PIC) (1,4). The N-terminal portion of the Gag cleavage product p12, a major constituent of the MLV PIC (5), associates with the capsid protein, thereby ensuring completion of reverse transcription and capsid core stability (6,7). During the cell cycle, this capsid core is maintained as an antiviral defense mechanism before mitosis (8). At the time of mitosis, phosphorylation of the S61 residue in the p12 protein disrupts the binding of the p12 N-terminus with its C-terminus, thereby facilitating capsid uncoating and revealing the p12 chromatin tethering motif (6–8). The MLV PIC is then tethered via its p12 C-terminal region to the chromosomes after nuclear membrane breakdown (5,9,10). In the nucleus, the viral complex is exposed to interactions with cellular cofactors such as the cellular bromodomain and extraterminal domain (BET) proteins (Brd2-4) (11–13). BET proteins target the MLV PIC to active enhancers at transcription start sites of genes, near CpG islands and DNaseI-hypersensitive sites (11–15). These proteins function as bimodal tethers, with the C-terminal ET domain directly interacting with the C-terminus of IN and the N-terminal bromodomains associating with promoter regions (11–13,16–18). Integration of the viral cDNA into the host cell chromatin is a hallmark of retroviral replication. Integration is mediated by the viral enzyme IN, a cleavage product of the Gag-Pol polyprotein, and occurs in two consecutive enzymatic reactions, called 3′-processing and strand transfer (ST) (19,20). MLV IN contains four domains: an

*To whom correspondence should be addressed. Tel: +32 0 11 26 92 13; Email: jelle.hendrix@uhasselt.be
Correspondence may also be addressed to Zeger Debyser. Tel: +32 0 16 33 21 83; Email: zeger.debyser@kuleuven.be
†The authors wish it to be known that, in their opinion, the three authors should be regarded as Joint Second Authors.

N-terminal domain (NTD) that coordinates a zinc ion and participates in the multimerization of IN, an internal catalytic core domain (CCD) containing the D,D(35)E motif that plays a key role in the catalysis of integration, and a less conserved C-terminal domain (CTD) involved in target DNA binding (21–23). Additionally, the MLV IN encodes an N-terminal extension domain required for MLV IN activity, with a possible role in interacting with host proteins (24,25).

While the enzymatic steps are well characterized, less is known about the role of the IN oligomeric state, and how this state evolves during nuclear entry and chromatin tethering and targeting steps. Various lines of evidence indicate that the catalytically active form of retroviral IN is an oligomer. For example, it has been long known that at least HIV-1 IN dimers are needed for catalyzing *in vitro* 3′-processing, and that at least a IN tetramer is necessary for concerted strand transfer (26–29). In recent years, structural characterization of the prototype foamy virus (PFV) revealed a functional IN tetramer (30,31), and structural studies of IN from the mouse mammary tumor virus (MMTV) and Rous sarcoma virus (RSV) revealed an octameric integrase architecture, composed of two core IN dimers and two flanking IN dimers (32,33). This quaternary structure is deemed to be a result of the limited linker length between their CCD and CTD domains. For HIV-1 and maedi-visna virus (MVV), two lentiviruses, having an intermediate linker length in IN, it has recently been shown that a range of oligomeric configurations are formed. These configurations range from a tetramer to higher order complexes (*e.g.* a homo-hexadecamer of IN for the MVV) formed via CTD rearrangements (34,35). For MLV IN, a tetramer has been proposed as the active form for concerted integration (22,23,36–39) and in fact, the length of the CCD-CTD linker in MLV IN is compatible with a tetrameric gammaretroviral intasome (32).

More recently, we used single-molecule fluorescence based analyses to reveal that the total IN content of HIV-1 PICs, as well as the quaternary structure of IN, functionally changes throughout the early stages of the replication cycle (40). More specifically, confocal laser scanning microscopy (CLSM) analyses showed a decrease in the number of IN molecules upon nuclear entry, and single-particle Förster resonance energy transfer (FRET) revealed how the host factor LEDGF/p75 altered the quaternary structure of the HIV-1 IN oligomer in the nucleus. A better understanding of the molecular mechanism of gammaretroviral MLV IN multimerization may explain how different retroviral families address the challenges of nuclear import and integration.

In this work, we investigated gammaretroviral Moloney MLV replication using single-molecule fluorescence approaches, by generating a fluorescent protein labeled version of the virus compatible with single-molecule FRET experiments. We followed the IN content and IN oligomeric state of the labeled INs in single viruses, and in viral complexes during early MLV replication. Our data show that the MLV PIC accesses the nucleus as a single, largely invariable complex. Clear changes in the IN oligomeric state are observed that are independent of p12-mediated tethering to metaphase chromosomes but closely linked to BET-mediated chromatin interaction.

MATERIALS AND METHODS

Plasmids

The MLV packaging plasmids coding for the MLV-IN-mTurquoise2, MLV-IN-mVenus and MLV-IN-mTurquoise2-mVenus proteins were constructed by digesting the corresponding plasmid coding for MLV-IN-eGFP (41) with *Nhe*I/*Not*I and replacing eGFP by the individual fluorescent protein mTurquoise2 or mVenus or the fusion construct mTurquoise2-mVenus, respectively. Genes of the fluorescent proteins were amplified by PCR with the following primers: 5′-GATCGCTAGCATGGTGAGCAA and 5′-GATCGCGGCCGCTCTTGTACA. The W390A and D184N mutations in the MLV-IN-FP constructs were introduced *via* site directed mutagenesis with the primer 5′-G GACCATCCTCTAGACTGACAGCGCGCGTTCAAC and 5′-CAGGCCCATTGTTAGTTCCCAATACCT, respectively. The original template was digested with *Dpn*I. To create MLV p12(PM14) (42), the WT p12 was replaced by a gene block fragment (Integrated DNA Technology, Belgium) encoding p12 with a five amino acids alanine block substitution (PM14) flanked by a *Sca*I and *Xho*I restriction sites. Both the gene fragment and the MLV-IN-mTurquoise2/V packaging constructs were digested with *Sca*I and *Xho*I to introduce the gene fragment in the packaging constructs.

Cell culture and synchronization

HEK293T (ATCC CRL-11268, Manassas, VA, USA) cells were cultured in Dulbecco's modified Eagle's medium (DMEM) (Life Technologies Europe, Merelbeke, Belgium) supplemented with 5% (V/V) heat inactivated fetal bovine serum (FBS; Life Technologies Europe) and gentamicin (50 μg/mL, Thermo Fisher, Erembodegem, Belgium). HeLaP4 cells (a kind gift from Pierre Charneau, Institut Pasteur, Paris, France) were cultured in DMEM supplemented with 2% (v/v) FBS, gentamicin (50 μg/ml) and geneticin (500 μg/ml, Gibco BRL). Both cell lines were grown in a humidified atmosphere with 5% CO_2 at 37°C. Cells were synchronized following an approach similar to the one discussed in Roe *et al.* (43). In brief, cells were seeded at an initial density of 2×10^4 cells per eight-well chambered coverglass (VWR international) or 2×10^5 cells per 24-well plate (Sigma-Aldrich, Bornem, Belgium) on day 1. On day 2, cells were serum starved by replacing the growth medium with DMEM containing 0.25% (v/v) FCS. On day 4, medium was replaced with DMEM containing 10% (v/v) FBS and cells were incubated for another 6 h. Thereafter aphidicolin (2 μg/mL) was added and 6 h later, the medium was removed and virus dilutions added for 2 h, after which the virus was removed and replaced with 10% (v/v) FBS containing medium.

Counting mitotic cells

For flow cytometry (Guava®easyCyte™ 5HT, Merck, Overijse, Belgium) HeLaP4 cells were harvested, washed

once with phosphate buffered saline (PBS) and fixed in 70% (v/v) ethanol for 2 h. Ethanol was removed by washing cells with PBS, and DNA staining was done by resuspending cells in 200 μl PBS containing 1× propidium iodide (20×, Sigma-Aldrich) and 1 mg/ml DNase-free RNase A (Sigma-Aldrich), and incubating for 20 min at 37°C in the dark. The percentage of cells in metaphase or G2 phase was determined using the FlowJo_V10 analysis software. We also used confocal microscopy to manually count the percentage of cells containing condensed, metaphase chromosomes using DAPI staining.

Retroviral vector production

Unless explicitly stated otherwise, gammaretroviral vectors were produced by a branched polyethyleneimine (bPEI; 10 μM, Sigma-Aldrich) transfection of 6.5×10^6 HEK293T cells per 10 cm petri dish with three plasmids: 7 μg pVSV-G envelope, 12.5 μg of the $MLV_{IN\text{-}FP}$ packaging plasmid (or any of its derived mutants) and 32.5 μg of the pLNC-fLuc3 transfer plasmid. Six hours post-transfection, the medium was replaced with OptiMEM (Life technologies) supplemented with 50 μg/ml gentamicin (Invivogen). Supernatant was collected 48 and 72 h post-transfection, filtered through a 0.45-μm filter (Sartorius) and the virus was concentrated by ultrafiltration (Vivaspin, MWCP 50K, Merck). Vector titers, represented as reverse transcriptase units (RTU), were determined by the SYBR Green-I product-enhanced reverse transcriptase assay (44) and shown as compared to the reverse transcription activity of a standard MLV stock. Subsequently, functional transducing titers were determined with viral vectors containing a pLNC-T2A-eGFP-fLuc instead of the pLNC-fLuc as standard, using FACS in 20 000 cells reaching $>5 \times 10^6$ TU/ml.

Vector transduction

HeLaP4 cells (2×10^5 cells/well) were seeded in eight-well chambered cover glasses (Nunc Lab-Tek chambered Coverglasses, 155411, Thermo Scientific) and subsequently synchronized using serum starvation and aphidicolin treatment, followed by transduction using the fluorescent MLV at a multiplicity of infection (MOI) of 25. After 2 h cells were washed and cultured for another 12 h (unless otherwise stated) in DMEM 10% (v/v) FBS after which the cells were fixed using 4% (v/v) paraformaldehyde. For dose-response experiments, raltegravir (RAL; 0.6 nM-600 nM), JQ1(+) (1–400 nM) or DMSO were added during transduction and during the 12 h following the vector incubation step. For immunocytochemistry, cells were permeabilized with 0.1% (v/v) Triton X-100 (Sigma-Aldrich) in PBS and stained for the nuclear lamina with lamin AC antibody (1/500 dilution, sc-7292, Santa Cruz biotechnology) and secondary goat anti-mouse Atto647N (1/500 dilution, Molecular probes, Thermo Fisher) diluted in blocking buffer: PBS containing 10% (V/V) FBS and 0.1% Tween-20 (V/V) (A4974, Applichem). DAPI staining was done using a 1/1000 dilution of a DAPI stock solution (Invitrogen). MLV Capsid staining of $MLV_{IN\text{-}Venus}$ was done using anti-MLV-p30 (rat monoclonal, Hybridoma R187 ATCC®-CRL1912™)

Compounds

When inhibitors RAL (NIH AIDS Reagent Program, Division of AIDS, NIH (Cat #11680) from Merck & Company, Inc) or the BET-protein-active compounds JQ1(+) and JQ1(−) were used, inhibitors were added during virus transduction for 2 h and during the 12 h following the vector incubation step. The BET-protein active compound JQ1(+) and inactive compound JQ1(−) were kindly provided by Prof. J. Bradner (Harvard University) and dissolved in DMSO (45).

Co-immunoprecipitation

For co-immunoprecipitation (coIP), 6.5×10^6 HEK293T cells were plated in 10 cm dishes and transfected using branched PEI (10 μM, Sigma-Aldrich) with 30 μg of the MLV-IN-V or MLV-IN(W390A)-V packaging construct. After 24 h, the cells were washed twice with PBS and lysed in whole cell lysis buffer (20 mM Tris–HCl pH 7.5, 250 mM NaCl, 1 mM $MgCl_2$, 0.5% (V/V) Triton X-100, 10% glycerol (v/v), 1 mM phenylmethanesulfonylfluoride (PMSF) and protease inhibitor cocktail (Complete: EDTA-free, 50×, Roche Diagnostics, Mannheim, Germany). Lysates were cleared by centrifugation at 20 000 g for 10 min and the supernatant was incubated overnight at 4°C with 3 μl of anti-GFP antibody (goat monoclonal antibody, ab6673, Abcam, Cambridge, UK). Subsequently, protein-G agarose (Roche Diagnostics) was added and samples were incubated at 4°C for 4 h. Samples were washed 5 times with coIP whole cell lysis buffer, before Western blot analysis.

Western blotting

Protein concentration of the supernatant from vector-producing cells was first determined using a bicinchoninic acid assay (BCA, Thermo Fisher Scientific, Geel, Belgium) after addition of 1% (w/v) SDS (Sigma-Aldrich). A total of 20 μg of protein was directly loaded onto 10% (w/v) polyacrylamide gels (Life technologies) for viral lysate experiments, or on a 4–15% precast gel (Criterion™ TGX™ Precast Midi Protein gel, BioRad, Nazareth, Belgium) for co-immunoprecipitation experiments. Proteins were electroblotted onto polyvinylidene difluoride membranes (PVDF, Bio-Rad laboratories, Nazareth Eke, Belgium). The following primary antibodies were used for western blot detection: anti-GFP (1/2500, goat monoclonal antibody, ab6673, Abcam, Cambridge, UK), anti-Gag (1/2500, rabbit polyclonal anti-MLV-Gag antibody, ab100970, Abcam), anti-CA (undiluted, rat monoclonal anti-MLV-p30/CA antibody, Hybridoma R187 ATCC®-CRL1912™, Manassas, Virginia, USA), anti-RT (undiluted, goat polyclonal anti-MLV-RT antibody, 76S-449, a kind gift from Dr Christine Kozak, NIH/NIAID) and anti-Brd4 (BET protein) (rabbit monoclonal antibody, A301–985A; Bethyl Laboratories, Antwerp, Belgium). Blots were subsequently stained with a horseradish peroxidase-conjugated goat anti-mouse, -rabbit, -rat or -goat antibody (Dako, Heverlee, Belgium) and detected by chemiluminescence (ECL^+, Amersham Bioscience, GE Healthcare Europe GmbH, Diegem, Belgium).

Luciferase assay

To determine the transduction efficiency of the vectors, 1.5×10^4 HeLaP4 cells were seeded per well in a 96-well plate and transduced the next day in triplicate in three dilutions in the absence or presence of RAL (0.6–600 nM) or JQ1(+) (1–400 nM) for dose response experiments. 24 h post-infection the vector was removed and replaced by DMEM containing 5% (v/v) FCS. To measure luciferase activity, cells were lysed 72 h after transduction in luciferase lysis buffer (50 mM Tris–HCl pH 7.5, 200 mM NaCl, 0.2% (v/v) NP-40, 10% (v/v) glycerol). Luciferase activity was measured following the manufacturer's protocol using ONE-Glo™ reagents (Promega, Leiden, The Netherlands). Luciferase activity was normalized for total protein content determined with a BCA assay. Subsequently, cells were split, and 50% was reseeded for luciferase assays or flow cytometry analysis, whereas the remaining 50% was kept in culture to determine integrated copies.

gDNA isolation and quantitative PCR

2.5×10^6 cells were pelleted, and genomic DNA was extracted using a mammalian genomic DNA miniprep kit (Sigma-Aldrich). Genomic DNA concentrations were determined using standard spectrophotometric methods. Samples corresponding to 100 ng genomic DNA were used for analysis. Each reaction contained 12.5 μl iQ Supermix (Biorad), 40 nM forward and reverse primer and 40 nM of probe in a final volume of 25 μl. The following primer/probes set were used: fLuc sense: 5′-TCACCCACACTGTGCCCATCTACGA and antisense: 5′-CAGCGGAACCGCTCATTGCCAATGG and probe: 5′-[6FAM]TTCATAGCTTCTGCCAACCGAACGGACA[TAM] and β-actin sense: 5′-GAAGAGATACGCCCTGGTTCC and antisense: 5′-TGTGATTTGTATTCAGCCCATATCG and probe: 5′-[6FAM]ATGCCCTCCCCCATGCCATCCTGCGT[TAM]. Samples were measured in triplicate for 5 min at 95°C followed by 50 cycles of 10 s at 95°C and 30 s at 55°C in a LightCycler480 (Roche Applied Science, Vilvoorde, Belgium). Analysis was performed using the LightCycler480 software supplied by the manufacturer.

Confocal microscopy and intensity analysis

Intensity measurements and imaging of cells was performed as described previously (40) using a laser scanning microscope (Fluoview FV1000, Olympus, Tokyo, Japan). The objective and the excitation polychroic mirror used were UPLSAPO 60× W NA1.2 and DM405–458/515/559/635, respectively (Olympus). 3D confocal stacks of fixed cells were acquired using a *z*-step size of 0.3 μm and sampling speed of 4 μs/pixel. A 440-nm diode laser was used for exciting mTurquoise2, a 514-nm diode laser for mVenus, a 405 nm laser for DAPI, and a 635-nm diode laser for Atto647N. Emission light was collected at 455-500 nm for mTurquoise2, 505–540 nm for mVenus, 430–470 nm for DAPI and 655–755 nm for Atto647N. The image resolution was 512 × 512 pixels and pixel size 103 nm. For dual or three-color images, different channels were combined for each *z*-plane and three consecutive *z*-planes were then assembled using ImageJ software (NIH). Detection, localization and intensity calculation for each IN-FP complex was performed as described previously using a homemade MATLAB routine (The MathWorks, Eindhoven, The Netherlands) (40). In brief, after image processing, particles were automatically detected using an intensity threshold. Each fluorescent spot that consisted of less than 7 pixels above the threshold was excluded. The remaining spots were assigned to be part of a single IN-FP complex if they were observed in at least 3 consecutive *z*-slices, with the complex at a maximum distance of 3 pixels (309 nm). Subsequently, the nuclear lamin was determined using intensity thresholding and used for automatic assignment of complexes to cytoplasm or nucleus while complexes in mitotic cells were manually selected. Next, the fluorescence signal of each complex in each *z*-slice was fitted with a 2D Gaussian using the least-mean-square method to calculate the integrated intensity of each IN-FP complex. Since the *z*-slice in which the complex is in focus is expected to have the highest intensity, this intensity value was selected for further use. Typically, data were collected from ∼50 different cells, which correspond to at least 300–1000 detected complexes per experiment. Each experiment was performed at least three times and data from a representative experiment are shown. The *P*-values for the intensity data are obtained from a two-sample *t*-test with unequal variance of the log-normal distributed data with *P*-value < 0.001 (***); $P < 0.01$ (**), $P < 0.05$ (*) and n.s. = not significant as the criterion of significance.

Quasi-TIRF microscopy and FRET analysis

Fluorescence imaging of the vectors for brightness analysis and FRET was performed as described previously (40). In brief, an inverted microscope (Olympus IX-83, Olympus NV) equipped with a TIRF oil objective (PlanApo 60 ×, NA1.45 oil TIRFM, Olympus). mTurquoise2 was excited at 445 nm (Cube 445-40c, Coherent, Utrecht, The Netherlands), eGFP was excited at 488 nm (Sapphire 488-100 CW, 100 mW, Coherent) and mVenus at 514 nm (Sapphire 514-100 CW CDRH, 100 mW, Coherent). Atto647N was imaged at 644 nm (Excelsior, Newport Spectra Physics BV, Utrecht, The Netherlands). After combining laser lines, the laser light was circularly polarized (WPQ05M-532, Thorlabs GmbH, Munich, Germany) and expanded 5 times to achieve a homogenous beam profile in the part of the sample that is imaged on the electron multiplying charge coupled device (EMCCD) chip and passed through a ∼1-cm iris to limit the illuminated area in the sample, before finally being focussed on the back focal plane of the objective through a 500-mm planoconvex achromatic lens (KPX211-C BK7 Precision Plano-Convex lens, Newport). Emission was collected by the same objective and split by a polychroic mirror (z445/514/633rpc, Chroma) into a blue emission channel for mTurquoise2 detection (HQ485/40m, Chroma), a yellow emission channel for mVenus detection (Razor Edge Long Pass 514 filter, Semrock, NY, USA) and a red emission channel for Atto647N detection (LP510 and LP655, Chroma). For eGFP, a polychroic mirror (z405/488/561/644rdc, Chroma) was used and emission light was detected using a HQ590/40–2P emission filter. The fluorescence image was expanded 2.5-

fold (PE eyepiece 125, 2.5 ×, Olympus) and focussed onto an EM-CCD (ImagEM, Hamamatsu, Louvain-La-Neuve, Belgium). The image size was 40 × 40 μm^2 and the image resolution 512 × 512 pixels. Images were acquired as the average of 20 consecutive 0.1 s integration time frames and the EM-gain was set to 191. FRET analyses were performed as described previously (40). In brief, single viral complexes ($MLV_{IN\text{-}mTq2+IN\text{-}mVenus}$) were localized by dual-color 2D Gaussian localization of the subdiffraction viral complexes (100-150 nm). Subsequently, the single particle integrated fluorescence intensity per virus of the FRET donor before ($F_{D,pre}$) versus after ($F_{D,post}$) photobleaching and of the FRET acceptor was extracted. Single-molecule localization/fitting was performed with Localizer (46). FRET was finally quantified by calculating the FRET ratio:

$$\text{FRET ratio} = \frac{F_{D,post}}{F_{D,pre}} \quad (1)$$

If FRET occurs between donor and acceptor, an increase of the donor fluorescence is observed after photobleaching of the acceptor. Typically, data were collected from ∼50–100 different cells, what correspond to an average of ∼200–2000 viral complexes per measurement. Each experiment was performed at least three times. From all the obtained FRET ratios, the average was taken and the standard error of the mean (SEM) was determined. Statistical analyses were performed with a Two-sample t-tests with unequal variance with the following *P*-value cutoffs: $P < 0.001$ (***); $P < 0.01$ (**), $P < 0.05$ (*) and n.s. = not significant.

TIRF microscopy *in vitro*

For fluorescence imaging of the vectors, virus-containing cell supernatants were diluted and immobilized onto 0.1% (w/v) poly-D-lysine (Sigma-Aldrich) coated wells in a 8-well chambered coverglass for 4 h at 37°C, washed with PBS buffer (Life technologies), fixed with 4% (v/v) paraformaldehyde (Sigma-Aldrich) in PBS, washed twice with PBS. Imaging was performed on the inverted TIRF microscope as described above and single viruses were localized by dual-color 2D Gaussian localization and the single particle integrated fluorescence intensity was determined. Single-molecule localization/fitting was performed with Localizer (46).

RESULTS

Functional MLV vectors for probing IN in single viruses

To investigate the IN content and oligomeric state during infection, we generated MLV genomic packaging constructs with the fluorescent protein (FP) genes mTurquoise2 (mTq2), mVenus (V) or eGFP, or a tandem fusion construct of mTq2 and Venus (mTq2-V), inserted in-frame downstream of the IN sequence and a short linker in the context of the complete Gag-Pol polyprotein (Figure 1A) (41). Fluorescently labeled vectors were produced in 293T cells by transient transfection of one ($MLV_{IN\text{-}mTq2}$, $MLV_{IN\text{-}V}$, $MLV_{IN\text{-}eGFP}$ or $MLV_{IN\text{-}mTq2\text{-}V}$) or two ($MLV_{IN\text{-}mTq2}$ and $MLV_{IN\text{-}V}$) packaging constructs, together with a commonly used transfer plasmid expressing firefly luciferase and a VSV-G envelope plasmid (Figure 1A).

Viral proteolytic processing was analyzed by Western blotting with specific antibodies against reverse transcriptase (RT; ∼71 kDa (47)) (Figure 1B), Gag (Supplementary Figure S1A), Capsid (CA) (Figure 1B, Supplementary Figure S1B), and eGFP (IN-eGFP ∼70kDa) (Figure 1B, Supplementary Figure S1A). In all conditions tested, CA was detected, confirming that proper Gag processing is preserved. Using the anti-RT serum three bands were visible, of which the topmost corresponds to full-length RT (∼71 kDa), as has been shown before (47). Finally, using the anti-GFP antibody, bands corresponding to the full-length IN fusion proteins were observed (∼70 kDa for IN-FP and ∼120 kDa for IN-mTq2-V), but a certain proportion was also present as cleaved products.

Next, we evaluated the transduction efficiency of the vectors using a firefly luciferase assay (Figure 1C). HeLaP4 cells transduced with equal amounts of vector as measured by reverse transcriptase activity, containing IN-mTq2, IN-V or both IN-mTq2 and IN-V produced a similar signal as the WT vector (no FP) (Figure 1C, Supplementary Figure S1C). These data imply that introduction of an FP C-terminally of Gag-Pol does not interfere with viral transduction efficiency. To control for the expression of the *fLuc* gene from non-integrated particles, we replaced IN with a catalytically dead version (D184N). As expected, three days after transduction of the host cells, only a limited luciferase activity was observed (Figure 1C). To assess the stability of vector integration, 293T cells were cultured until 10 days post-transduction, and the number of total vDNA copies was determined by quantitative PCR. This demonstrated stable integration of the transfer gene by fluorescently labeled MLV vectors (Figure 1D).

Next, we visually confirmed the presence of the FP in the vectors (Figure 1E). To this end, we coated microscopy coverslips with the supernatant of 293T cells that produced $MLV_{IN\text{-}V}$ at concentrations that allowed individual virus discrimination and immunostained the sample with the anti-CA antibody. Total internal reflection fluorescence (TIRF) microscopy was performed revealing that about 70 ± 10% of IN-Venus positive spots also positively stained for CA and 62 ± 12% of the CA-positive spots were also positive for IN-Venus (Figure 1E).

Finally, we also carried out an extensive comparative analysis of the different fluorescent protein tags (eGFP vs. mTurquoise2 vs. mVenus) in the context of single-labeled vectors, using a strategy similar as in Figure 1E, and for which the Reader is referred to Supplementary Figure S2. In brief, although virus production efficiency did scale with the MLV genomic plasmid concentration used (Supplementary Figure S2A, B), the IN content did not change (Supplementary Figure S2C, D). Overall, mVenus seemed the optimal tag for single-virus imaging, since most fluorescent moieties per virus were observed for $MLV_{IN\text{-}V}$ particles.

Taken together, we constructed MLV vectors with wild-type function carrying labeled IN protein.

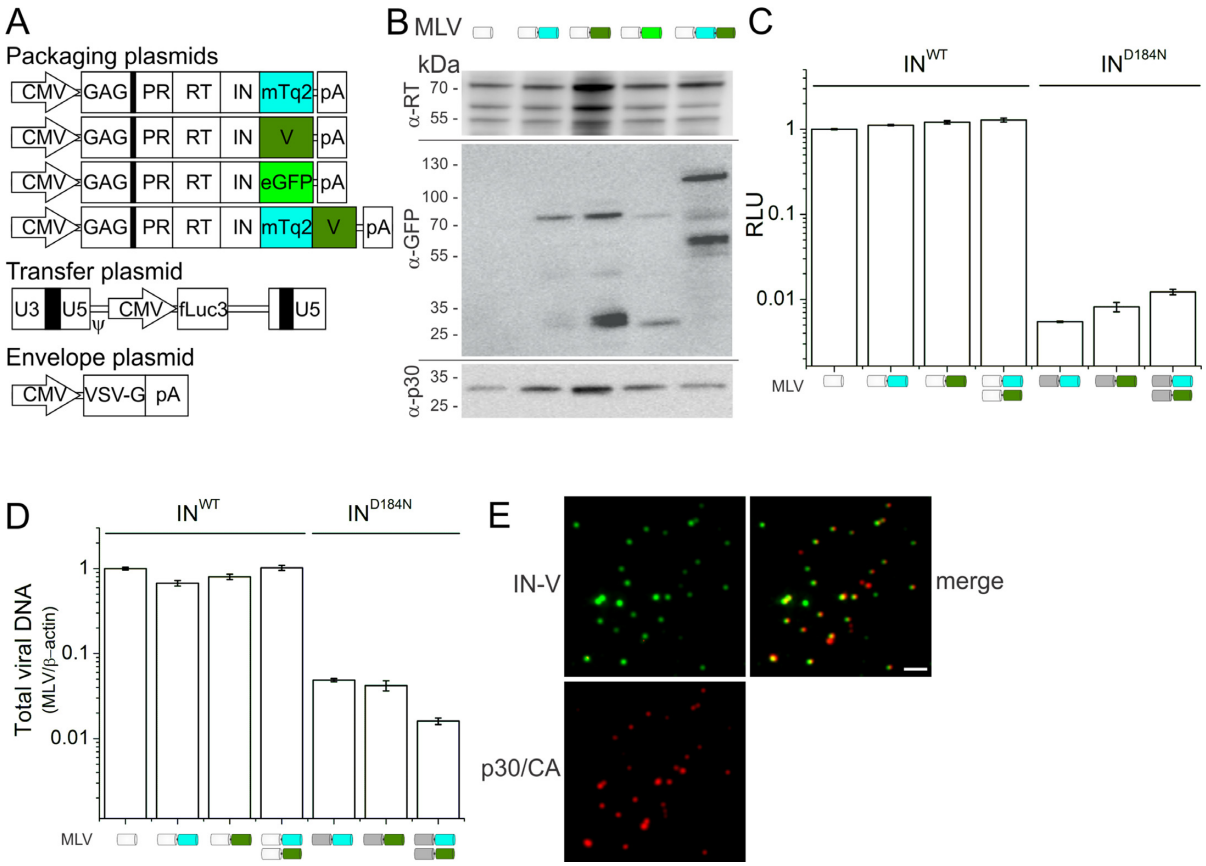

Figure 1. Functional MLV vectors for single virus imaging. (**A**) Schematic representation of the constructs used for MLV particle production: the packaging plasmids with the *pol* gene fused to a single mTurquoise2 (mTq2), mVenus (V) or eGFP fluorescent protein gene, or to a tandem heterodimer mTurquoise2-Venus (mTq2-V) fluorescent protein fusion gene, the transfer plasmid with a *Firefly luciferase* gene (fLuc3) and the VSV-G envelope plasmid. CMV = cytomegalovirus promoter, thick black line = in-frame suppression, PR = protease, RT = reverse transcriptase, IN = integrase, pA = poly-adenylation signal. (**B**) Western blot showing the presence of IN-FP, RT and CA in purified MLV particles. Vectors were analyzed with an antibody against (top) reverse transcriptase (anti-RT), (middle) mTurquoise2, mVenus, eGFP or the fusion construct mTq2-V (anti-GFP) and (bottom) CA (anti-p30). Extra data in Supplementary Figure S1A. (**C**) Firefly luciferase assay for testing the reporter gene expression of the fluorescently labeled vectors in HeLaP4 cells 3 days post-transduction. Vector amounts were normalized on particle-associated RT activity before transduction. Relative luminescence units (RLU) were normalized to the protein content of infected cell lysates. The bar chart (displayed in a log10 *y* scale) shows the average of a representative experiment performed in triplicate. Error bars indicate the standard deviation on triplicate data points. Extra data in Supplementary Figure S1B. (**D**) Bar chart (displayed in a log10 *y* scale) of the normalized total viral DNA (to β-actin) as determined via quantitative PCR in transduced 293T cells 10 days post transduction. Error bars indicate the standard error on the mean on triplicate data points. (**E**) TIRF microscopy image of $MLV_{IN\text{-}V}$ vectors (green) immunostained with anti-CA (red, Alexa633). The merged image shows CA/IN-FP colocalizing particles (yellow). The scale bar is 5 μm.

MLV IN oligomerizes inside MLV vectors

Different retroviral INs have previously been shown to functionally oligomerize in vitro (23,27–29,36,48–52). Recently, we corroborated this inside individual virions and viral complexes in HIV infected cells by single-molecule fluorescence experiments (40,53). We now employed our dual-color fluorescent MLV virions ($MLV_{IN\text{-}mTq2+IN\text{-}V}$), containing IN-mTq2 and IN-V in a 1:1 (plasmid) ratio to verify IN oligomerization via single-molecule Förster resonance energy transfer (FRET) experiments. More specifically, we used the increase in FRET donor (mTurquoise2 FP) fluorescence after FRET acceptor (mVenus FP) photobleaching as a measure for the presence and quaternary structure of IN oligomers (Figure 2A). Practically, we separately imaged the donor (D,pre; Figure 2A) and acceptor (A,pre; Figure 2A) labels at low laser power. Subsequently, the acceptor was photobleached at high laser power and the donor (D,post; Figure 2A) was imaged again. From the localized and 2D-Gaussian fitted spots in the fluorescence images (D,pre; A,pre and D,post), the single particle intensity was determined (Figure 2A), from which the FRET ratio per MLV-derived particle was calculated (Equation 1) and plotted (Figure 2B and Supplementary Table S1). We observed a percentage of particles containing a fluorescent FRET donor, that also contained a fluorescent FRET acceptor, equal to 78 ± 2% (Figure 2A; yellow). A FRET ratio of 1.25 ± 0.01 was obtained, which was significantly higher than the negative control, i.e. viruses containing only IN-mTq2 (1.03 ± 0.02). This suggests the presence of interacting IN subunits (Figure 2B). For a direct fusion between the donor and acceptor ($MLV_{IN\text{-}mTq2\text{-}V}$), the mean FRET ratio was 1.83 ± 0.02. Here, very efficient FRET is occurring between the donor and acceptor probes because of their close proximity. To rule out aspecific FRET signals, we repeated the experiment with $MLV_{IN\text{-}mTq2}$ vectors produced

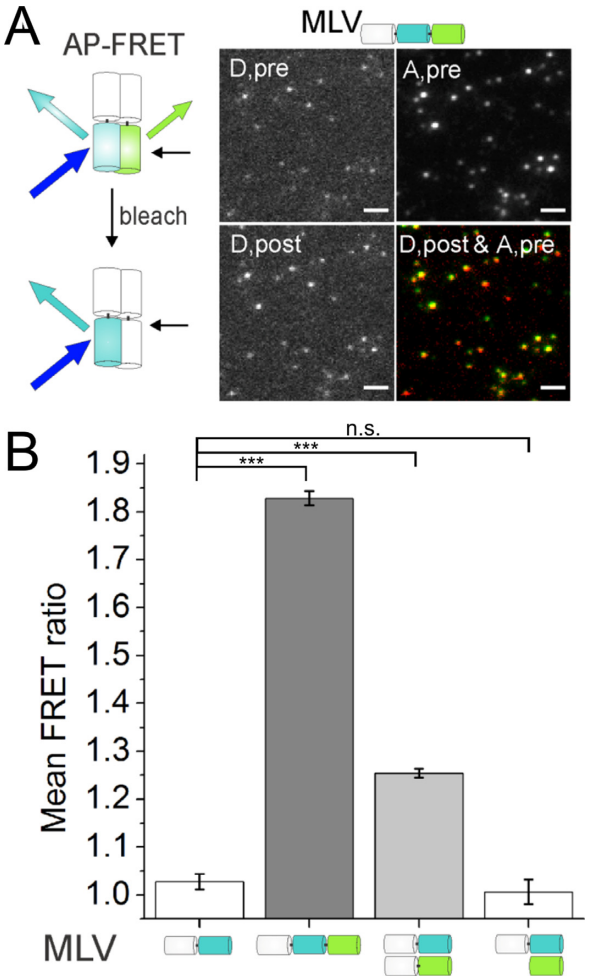

Figure 2. FRET picks up the IN quaternary structure. (**A**) $MLV_{IN\text{-}mTq2+IN\text{-}V}$ vectors are imaged in the FRET donor (D,pre) and acceptor (A,pre) detection channels at low laser power, after which the acceptor is photobleached at high laser power. Finally, the donor is imaged again in the blue channel at low laser power (D,post). Dual-color labeled particles are shown in yellow (IN-mTq2, red; IN-V, green). Scale bar is 1 μm. (**B**) Mean FRET ratios of MLV-derived particles containing only a donor FP ($MLV_{IN\text{-}mTq2}$), a FRET-pair fusion construct ($MLV_{IN\text{-}mTq2\text{-}V}$), two fluorescently labeled INs ($MLV_{IN\text{-}mTq2+IN\text{-}V}$) or only a donor fluorescently labeled IN and a free acceptor fluorescent protein ($MLV_{IN\text{-}mTq2+free\ V}$). *** $P < 0.001$; n.s. = not significant, from an unpaired Student's *t*-test with unequal variance.

in cells overexpressing free mVenus. In double-labeled particles, $MLV_{IN\text{-}mTq2+free\ mVenus}$, containing IN-mTq2 and free mVenus, no increased FRET ratio (1.01 ± 0.03) was observed (Figure 2B), excluding an aspecific FRET artifact under the experimental conditions.

Together, these experiments show that the FRET signal in $MLV_{IN\text{-}mTq2+IN\text{-}V}$ vectors originates from oligomerization of the fluorescently labeled IN. This is the first time IN oligomers are observed directly at the level of a functional MLV vector without the need for lysis of the MLV-derived particles. In a next step, we employed the described single-virus FRET assay to investigate the IN quaternary state inside individual viral pre-integration complexes (PICs) during transduction.

Nuclear presence of FP-labeled MLV PICs depends on the cell cycle and viral integration

Gammaretroviruses such as MLV require cell cycle-dependent nuclear membrane breakdown to gain access to the host cell DNA prior to integration (1,2,43). To increase the likelihood of observing interphase cells carrying nuclear fluorescent MLV PICs, we synchronized the cells by releasing them from an aphidicolin based cell cycle arrest at the G_1/S border (the Reader is referred to Supplementary Figure S3A for a scheme of the cell cycle) at the moment of investigation. We used two complementary methods to monitor the cell cycle: visual inspection of metaphase (M) cells (Figure 3A) and flow cytometry (Figure 3B and Supplementary Figure S3B). After removing aphidicolin at time zero, an increased percentage of G2/M phase cells was observed starting at 8 h and peaking at 14 h (Figure 3B). At 14–16 h, approximately 7% of cells were in metaphase (Figure 3A).

In a next set of experiments, we employed single-color labeled MLV particles containing IN-mVenus to study MLV PICs during the early replication steps. Upon transduction of the synchronized cells, clearly punctuate fluorescent spots were readily detected in the cytoplasm of the target cells (Figure 3C, interphase). Upon nuclear envelope breakdown and chromosome condensation (Figure 3C, prometaphase until telophase) fluorescent viral complexes overlapped with the chromosomes, as has been shown before (9,41). For cells that had gone through mitosis post-transduction, the large majority of viral complexes (90 ± 4%) were located inside the nucleus (Figure 3C, post-mitotic interphase) and overall, the percentage of cells containing nuclear viral complexes increased with the progression through the cell cycle (Figure 3D, E), peaking at 15 h post–transduction. The transduced mitotic or post-mitotic cells contained about 20 viral complexes in the 8–20 h time span (Figure 3F), which corresponds to the employed multiplicity of infection (MOI = 25). When aphidicolin was not removed at time zero, a much lower percentage (<5%) of cells with nuclear MLV complexes was observed at 14 h (Figure 3E). The presence of fluorescent complexes tethered to mitotic chromatin and the cytosolic retention of PICs upon aphidicolin treatment corroborate previous findings on nuclear migration of MLV PICs (43).

At later time points (>15 hours), the percentage of cells with nuclear viral complexes decreased (Figure 3D), a trend that was also reflected by the number of nuclear PICs at 30 h after infection (Figure 3F). The decrease can be due to proviral integration and subsequent PIC dissociation, integration-independent PIC dissociation, dilution through subsequent mitosis events or active breakdown by the cellular housekeeping machinery. To investigate this further, we added the integrase strand transfer inhibitor raltegravir (RAL) during transduction. Relative to the DMSO control, an increased number of cells containing nuclear PICs was observed (Figure 3G). This strongly suggest that the observed reductions in cells containing nuclear PICs and nuclear PICs per cell following the first cell division is, at least in part, due to integration of functional intasomes and concomitant PIC dissociation post-integration.

In summary, the percentage of cells containing nuclear PICs, and the number of PICs in the nucleus of post-mitotic

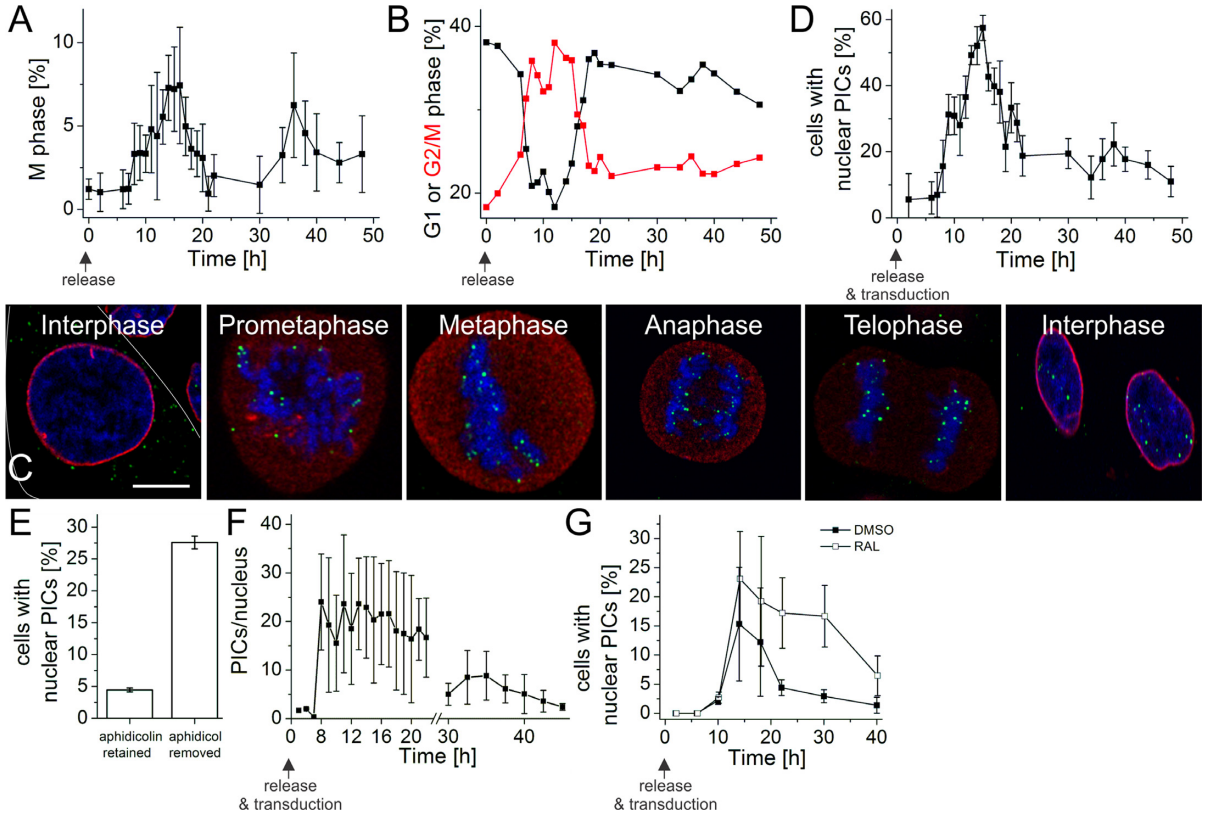

Figure 3. Nuclear presence of fluorescent MLV PICs depends on the cell cycle and integration. (**A**) Percentage of metaphase cell counted via confocal microscopy. Twenty fields of view were counted and expressed as percentage of metaphase cells. (**B**) Percentage of HeLaP4 cells in G1 (black) or G2/M phase (red) as determined with flow cytometry. Indicated hours are relative to the time of transduction, when cells were first exposed to the MLV vectors after lifting the prior arrest at G_1/S with serum starvation and aphidicolin treatment. For clarity, data in panel B was smoothed by phase-conserving averaging over three time points. Raw flow cytometry data are in Supplementary Figure S3B. (**C**) Confocal images of HeLaP4 cells during the cell cycle following transduction at time zero with $MLV_{IN\text{-}V}$ vectors (green). Cells were immunostained using antibodies recognizing the nuclear lamin (red) and the chromatin was stained with DAPI (blue). Scale bar is 5 μm. (**D**) Time course to determine when synchronized and transduced cells contain the most nuclear MLV PICs. A minimum of 50–100 cells was scored under each condition. (**E**) Percentage of cells with nuclear PICs at 14 h when aphidicolin was removed or retained during transduction with $MLV_{IN\text{-}V}$ at 0 h. As panels D and E illustrate independent experiments, the absolute numbers differ. (**F**) The average number of nuclear MLV PICs in HeLaP4 transduced with $MLV_{IN\text{-}V}$ over a period of 48 h post transduction. (**G**) Time progression of the percentage of HeLaP4 cells with nuclear viral complexes after transduction of $MLV_{IN\text{-}V}$ in the presence of DMSO or RAL (0.6 μM). For the 22, 30 and 40 hour time points, the Student's *t*-test with unpaired variance *P* values were $P < 0.01$ when comparing the DMSO and RAL data.

cells closely followed the cell cycle, and appeared to be, at least in part, dependent on viral integration.

Cytoplasmic and nuclear PICs differ in IN quaternary structure, but not in IN content

We next probed the IN content of intracellular viral complexes relative to that of the vectors. We observed a slight decrease in Venus intensity upon entry of the virus into cells, yet comparable intensities between cytoplasmic, chromosome-bound (metaphase) and (post-mitotic) nuclear IN-mVenus complexes (Figure 4A, B and Supplementary Table S2). As this decrease did not depend on the subcellular location (data not shown), nor time post transduction (data not shown), this may suggest the presence of non-specific/-functional IN-FP (or even free FP) moieties in the virions, that are lost immediately upon cell entry.

As comparable fluorescence intensities were observed for cytoplasmic, chromosome-bound and nuclear complexes, we next assessed a possible correlation between viral CA and IN content. More specifically, we used immunofluorescence to compare the colocalization of IN-V with CA in $MLV_{IN\text{-}V}$ transduced cells in different phases of the cell cycle (Figure 4C, Supplementary Figure S3A). Both proteins colocalized in viral complexes early during infection (Figure 4C, interphase). For the majority of particles, a clear overlap (63 ± 21% of IN-V spots also stained for CA, 72 ± 19% of CA spots also stained for IN-V) was observed in the cytoplasm of interphase cells, as calculated from 81 cells containing 10–30 viral complexes (Figure 4D). This is similar to the colocalization observed *in vitro*, for virus particles that were simply absorbed to glass coverslips (Figure 1E). Complexes bound to mitotic chromosomes displayed a much-decreased overlap (only 1.7 ± 0.5% of IN-V spots stained for CA, 7 ± 0.4% of CA spots stained for IN-V) (Figure 4C, Metaphase/Telophase and Figure 4D, middle bar). Furthermore, in post-mitotic interphase cells (Figure 4C, Post-mitotic interphase and Figure 4D, right bar; 0 ± 0%), no significant overlap between CA and IN-FP was observed. These results imply that capsid uncoating from intasomes occurs before binding to the condensed chromo-

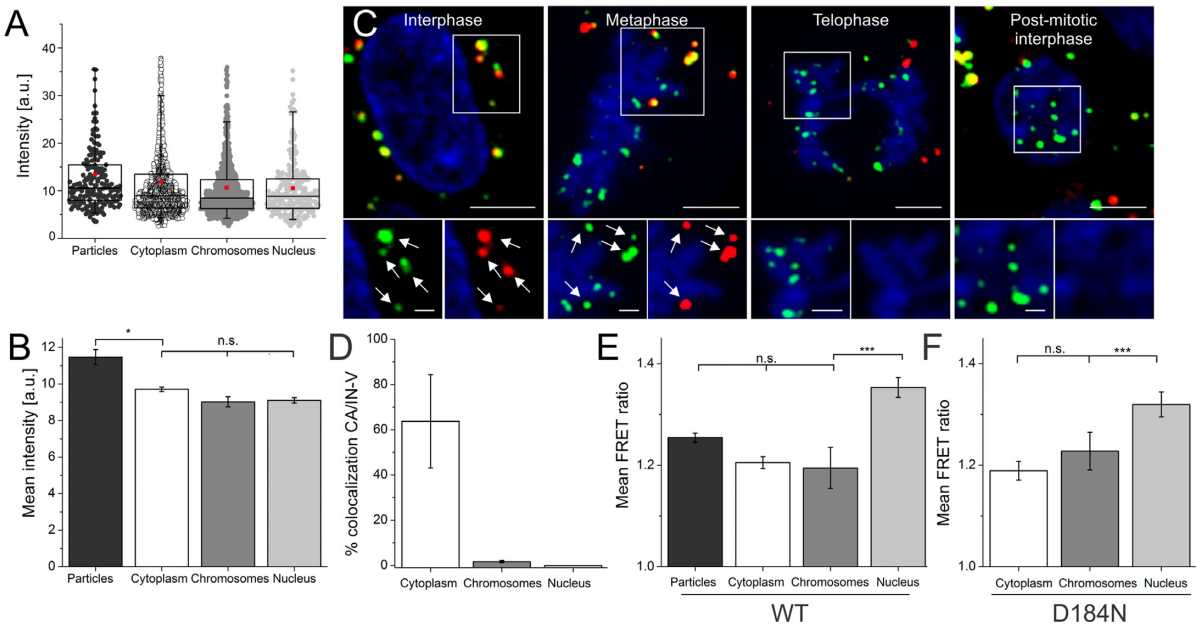

Figure 4. IN quaternary structure is reshaped after mitosis. (**A**) Fluorescence intensity, and (**B**) mean intensity of $MLV_{IN\text{-}V}$ vectors (dark gray) or viral complexes at t = 14 h post-transduction in synchronized HeLaP4 cells in the cytoplasm (white), bound to chromosomes (gray) or in the nucleus of post-mitotic interphase cells (light gray). Box-plot whiskers in panel A represent the 5th and 95th percentiles, the median value is represented by a horizontal line, and the red square is the mean fluorescence intensity. Error bars represent standard error of the mean (SEM); $*P < 0.05$; n.s. = not significant, from an unpaired Student's *t*-test with unequal variance. (**C**) False-colored confocal images of HeLaP4 cells transduced with $MLV_{IN\text{-}V}$ vectors, displaying IN-V (green), immunostained CA (red) and DAPI (blue). Magnifications are shown next to the image. Scale bars are 5 μm (magnifications 2 μm). White arrows point towards localized spots that were localized in both IN-FP and CA imaging channels. (**D**) Percentage of colocalization of IN-V and CA for viral complexes in the cytoplasm, bound to chromosomes or in the nucleus of post-mitotic interphase cells, calculated from 130 cells, each containing 10–30 MLV viral complexes. (E, F) Mean FRET ratios in HeLaP4 cells synchronized using serum starvation and aphidicolin treatment, followed by transduction with (**E**) $MLV_{IN\text{-}mTq2+IN\text{-}V}$ or (**F**) $MLV_{IN(D184N)\text{-}Tq2+IN(D184N)\text{-}V}$ complexes at $t = 14$ h in the cytoplasm (white), bound to chromosomes (gray) or in the nucleus of post-mitotic interphase cells (light gray) compared to $MLV_{IN\text{-}mTq2+IN\text{-}V}$ vectors (black). Error bars represent the standard error of the mean (SEM); $***P < 0.001$; n.s. = not significant, from an unpaired Student's *t*-test with unequal variance.

somes during mitosis, as suggested before (9) and has no influence on the IN content.

Finally, we monitored the interaction between labeled IN subunits in viral complexes in the cell. A FRET ratio of 1.20 ± 0.01 was measured for cytoplasmic MLV complexes before mitosis, much like the value obtained for IN oligomers inside MLV-derived particles (Figure 4E and Supplementary Table S3). Remarkably, whereas MLV complexes bound to chromosomes in metaphase cells displayed a similar FRET ratio of 1.20 ± 0.04, the FRET ratio of post-mitotic nuclear MLV complexes was significantly higher (1.35 ± 0.02), directly implying a quaternary structure change of IN. Furthermore, viruses incorporating the IN(D184N) mutation ($MLV_{IN(D184N)\text{-}Tq2+IN(D184N)\text{-}V}$), that catalytically inactivates IN (54), still exhibited wild-type FRET levels. Together, these data show that the interaction with chromosomes as such, nor the catalytic activity of IN, affects the IN oligomer although completion of mitosis is required for the process to occur (Figure 4E).

In conclusion, the CA colocalized with IN-FP in cytoplasmic PICs in interphase cells, but colocalization was significantly lower for PICs docked to mitotic chromosomes, as well as for PICs in the nucleus after nuclear envelope reassembly. CA uncoating was not associated with a drop in fluorescence intensity (IN content). Rather, the quaternary structure (stoichiometry and/or conformation) of the MLV IN oligomer did undergo significant alterations in the nucleus of post-mitotic interphase cells independent of the catalytic activity of the integrase.

BET protein-dependent change in IN oligomeric state in post-mitotic nuclear viral complexes

Alteration of the IN-FP oligomeric state may be due to the interaction of p12 in the PIC with post-mitotic chromatin, to the interaction of MLV IN with the host factors Brd2-4, known to tether MLV IN to the chromatin, or to the integration event itself (Figure 5A). To address this question, we first investigated the role of p12, a cleavage product of the MLV Gag precursor and a component of MLV PICs (5). MLV p12 is known to bind to the condensed chromosome via its C-terminal region, thereby tethering the MLV PIC to the host chromosomes (9,10). In addition, the p12 N-terminal region is known to interact with the MLV capsid, thereby stabilizing the capsid core of the MLV PIC complex and preventing premature capsid uncoating (6–8). About 89 ± 5% of PICs containing WT p12 accumulated on mitotic chromosomes (Figure 5B; top). Chromosome accumulation of PICs with a mutant p12 protein PM14, *i.e.* a five-amino acid alanine block substitution (42), on the other hand, was severely impaired (only 11 ± 2% of PICs overlapped with chromatin) (Figure 5B; bottom) (5). In cells transduced with $MLV_{IN\text{-}mTq2+IN\text{-}V,p12(PM14)}$, much less post-mitotic nuclear MLV complexes were also found (7 ± 4% in comparison to

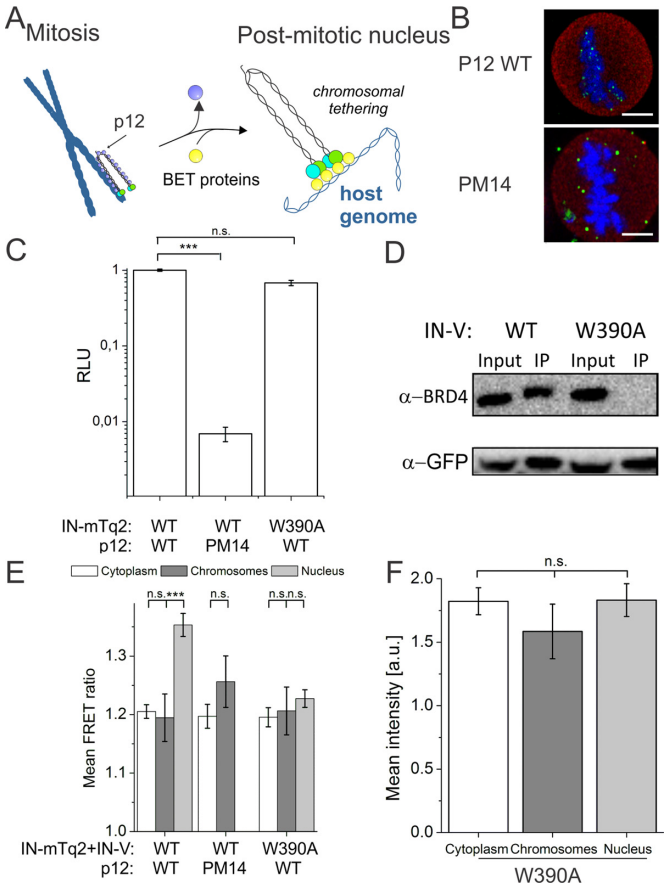

Figure 5. Interaction with BET proteins is essential for IN quaternary structure change. (**A**) Currently accepted MLV PIC tethering model. Upon nuclear reassembly after mitosis, the viral protein p12 chromosome (purple circles) tether dissociates, and BET proteins (yellow circles) take over, readying the chromatin associated PIC (with IN-FP proteins indicated by green and cyan circles) for integration (9,11–13). (**B**) Confocal images of cells in metaphase transduced with $MLV_{IN\text{-}V}$ or $MLV_{IN\text{-}V,p12(PM14)}$ vectors (green), immunostained using antibodies recognizing the nuclear lamin (red) and stained with DAPI for DNA (blue). Scale bars are 5 μm. (**C**) Bar chart (displayed in a $\log_{10}$ y scale) illustrating the results of a firefly luciferase assay testing the transduction efficiency of $MLV_{IN\text{-}V}$, $MLV_{IN\text{-}V,p12(PM14)}$ or $MLV_{IN(W390A)\text{-}V}$ vectors. Vectors were normalized on RT activity before transduction. Relative light units (RLU) were normalized for protein content of the transduced cell lysates. Results show a single experiment performed in triplicate. (**D**) Co-immunoprecipitation of endogenous Brd4 with transiently expressed packaging constructs containing the FP-tagged MLV WT IN protein (IN-V) or the W390A mutant IN(W390A)-V protein analyzed by western blot. (**E**) Mean FRET ratio of $MLV_{IN\text{-}mTq2+IN\text{-}V}$, $MLV_{IN\text{-}mTq2+IN\text{-}V,p12(PM14)}$ or $MLV_{IN(W390A)\text{-}mTq2+IN(W390A)\text{-}V}$ viral complexes at t = 14 h post-transduction in synchronized HeLaP4 cells. (**F**) Mean fluorescence intensity of $MLV_{IN(W390A)\text{-}V}$ viral complexes at t = 14 h post-transduction in synchronized HeLaP4 cells. (E, F) Complexes are in the cytoplasm (white), bound to chromosomes (gray) or in the nucleus of post-mitotic interphase cells (light gray). Error bars represent the standard error of the mean (SEM); ***$P < 0.001$; n.s. = not significant, from an unpaired Student's t-test with unequal variance.

90 ± 4% with WT p12), consequently resulting in a highly reduced transduction efficiency (Figure 5C). These results thus confirm that binding to chromosomes during mitosis is a prerequisite for nuclear retention after mitosis.

Next, we investigated the effect of the p12 mutation on the IN quaternary structure. The FRET ratio obtained for the cytoplasmic and metaphase chromosome-bound complexes containing the p12 mutation was similar as the value for WT MLV vectors (Figure 5E), suggesting that the increase in FRET can only occur after retention in newly formed nuclei. Since the mutation of p12 prevented nuclear retention post-mitosis almost completely, its direct impact on the FRET ratio could not be quantified (Supplementary Table S3). Nonetheless, this result, together with the fact that the (IN-)FP and CA colocalized in cytosolic and mitotic (chromatin-bound) PICs, and almost not in (post-mitotic) nuclear PICs (Figure 4C, D), implies that the FRET increase takes place after dissociation of both CA and p12 from the PIC. This timely dissociation may expose the complex to interactions with cellular proteins, as already suggested by Elis *et al.* (9).

Previously, we showed that LEDGF/p75, the tethering and targeting factor of HIV integration (55) is responsible for changing the oligomeric state of HIV-1 IN in the nucleus (40). To exclude a role of LEDGF/p75 in the observed FRET increase for fluorescent MLV particles, we transduced LEDGF/p75-depleted HeLaP4 ($LEDGF/p75^{KD}$) with $MLV_{IN\text{-}mTq2+IN\text{-}V}$ and quantified the FRET ratio. This resulted in a similar FRET increase in nuclear MLV IN complexes as observed in the wild-type HeLa P4 cells (Supplementary Figure S4).

We next investigated the effect of the BET proteins (Brd2-4), recently shown to function as MLV integration targeting factors (11–13,17), analogously to the role of LEDGF/p75 in HIV-1 replication. As a knock down of all three Brd proteins (Brd2-4) is toxic to the cell (13), we opted to introduce a single point mutation (W390A) in MLV IN. Using alanine scanning this residue had previously been shown to be critical for the interaction of IN with the ET domain of the BET proteins (11,17), and W390A has been shown to redistribute integration away from transcription start sites (TSS) and CpG islands (56,57). Indeed, and as observed before, a single W390A substitution did not result in a significant transduction loss (Figure 5C).

All BET proteins (Brd2-4) predominantly interact with the 28 C-terminal amino acids of MLV IN (11,13,17). Therefore, and as a control to confirm that introduction of an FP at the C-terminus of MLV IN does not impair its interaction with Brd4, we performed a co-immunoprecipitation experiment in 293T cells transiently expressing IN-V or IN(W390A)-V. Brd4 was readily detected in the extracts of cells transfected with IN-V, but not with IN(W390A)-V coding constructs (Figure 5D), confirming a similar interaction of Brd4 with WT IN and IN-V. Conversely, in contrast to $MLV_{IN\text{-}Tq2+IN\text{-}V}$, the FRET ratio of $MLV_{IN(W390A)\text{-}Tq2+IN(W390A)\text{-}V}$ did not increase in the post-mitotic nucleus (Figure 5E), indicating that BET proteins (Brd2-4) are required for the observed FRET phenotype. We corroborated that the W390A mutation did not result in an overall altered IN oligomerization behavior via DTSSP crosslinking and Western blotting of nuclear extracts of MLV IN transfected cells (Supplementary Figure S5), as well as via an AlphaScreen oligomerization assay (Supplementary Figure S6). Also, comparable fluorescence intensities, and thus IN moieties per viral complex, were observed between cytoplasmic, chromosome-bound (metaphase) and (post-mitotic) nuclear $MLV_{IN(W390A)\text{-}V}$ complexes (Figure

5F), similar as for the WT vector (Figure 4B). Together, these experiments imply that the absence of an increased nuclear FRET signal for the W390A mutant relates to a structural change within the viral complex, rather than to a concentration related artifact or oligomerization defect.

Together, these results show that the p12 protein is required for efficiently transducing MLV vectors by allowing the virus to localize in the post-mitotic nucleus, and that only a specific BET-IN interaction can elicit the observed IN quaternary structure change.

Bromodomain inhibitors and RAL interfere with MLV IN oligomerization

The bromodomain inhibitor compound JQ1(+) selectively inhibits interactions of all three BET proteins with cognate-modified histone sites (45), effectively displacing BET proteins from chromatin (58) and thereby inhibiting MLV integration into transcription start sites (Figure 6A) (11–13). We investigated the effect of JQ1(+) on the change in IN quaternary structure. Based on the 50% cytotoxicity (CC_{50} = 0.652 μM) and inhibitory concentrations (IC_{50} = 0.122 μM) as determined in De Rijck *et al.*, we used a JQ1(+) concentration of 200 nM, at which at least a two-fold inhibition is expected (11). As a negative control we included 200 nM of JQ1(–), the inactive R-enantiomer of JQ1(+). HeLaP4 cells were transduced with the $MLV_{IN\text{-}mTq2+IN\text{-}V}$ vector in the presence of either JQ1(-) or JQ1(+). Interestingly, JQ1(+), but not JQ1(–), prevented the nuclear FRET increase of MLV IN complexes (Figure 6B), indicating that interaction between the BET proteins and chromatin is additionally required for the increased FRET in the post-mitotic nucleus. We also evaluated whether JQ1(+)-induced inhibition of FRET increase correlated with a reduction in infectivity by adding 1–400 nM of JQ1(+) in both FRET and infectivity assays (Figure 6C, D). Inhibition of the nuclear FRET increase was observed at 50 nM (Figure 6C, gray bars), and this inhibition closely correlated with the luciferase infectivity assay (Figure 6D).

We next wondered whether direct interactions of IN with chromatin are needed to trigger the observed IN structural rearrangements. The IN strand transfer inhibitor RAL binds to functional intasomes close to the 3′-end of the viral DNA, thereby competing with IN target DNA binding (59). Similar to JQ1(+), RAL prevented the FRET ratio increase in a dose-dependent manner (0.6–600 nM) (Figure 6E). This inhibition correlated again with the inhibition of transduction of $MLV_{IN\text{-}mTq2+IN\text{-}V}$ vectors (Figure 6F). Finally, no further decrease in the FRET signal was observed when the $MLV_{IN(W390A)\text{-}Tq2+IN(W390A)\text{-}V}$ vectors were used in combination with RAL (600 nM) or JQ1(+) (200 nM) (Supplementary Figure S7).

On the one hand, these experiments strengthen our hypothesis that the nuclear FRET increase of the virus, and concomitant quaternary structure change of the virus, is important for viral fitness and infectivity, and can thus be used as such to investigate the viral infection mechanism. Mechanistically, these results imply that only the ternary complex of BET proteins, chromatin and IN allows for a specific structural rearrangement within the IN complex. These rearrangements might eventually determine the integration sites preferred by the MLV such as CpG islands and transcription start sites.

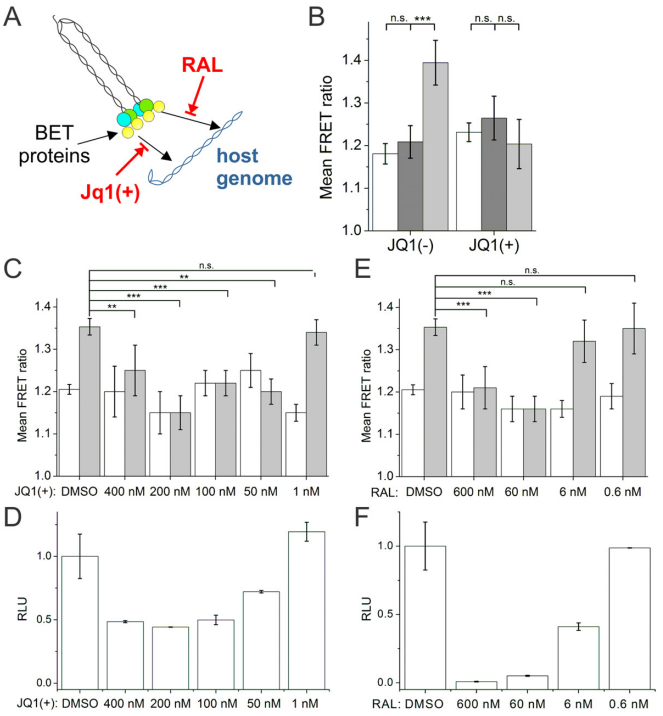

Figure 6. Host genome docking precedes MLV PIC quaternary structure changes. (**A**) Currently it is accepted that RAL binds functional intasomes and inhibits target DNA binding, while JQ1(+) abolishes the interaction between BET proteins and the chromatin (45,58,59). (**B**) HeLaP4 cells were synchronized using serum starvation and aphidicolin treatment, followed by transduction in the presence of (B) JQ1(–) or JQ1(+). Mean FRET ratios from $MLV_{IN\text{-}mTq2+IN\text{-}V}$ viral complexes were determined at t = 14 h post-transduction in synchronized HeLaP4 cells in the cytoplasm (white), bound to chromosomes (gray) or in the nucleus of post-mitotic interphase cells (light gray). (**C–F**) Synchronized HeLaP4 cells were transduced with $MLV_{IN\text{-}mTq2+IN\text{-}V}$ complexes in the presence of varying concentrations of (C, D) JQ1(+) (1–400 nM), (E, F) RAL (0.6–600 nM) or DMSO. (C, E) FRET readouts in the cytoplasm (white) or in the nucleus (light gray) of post-mitotic interphase cells at t = 14 h post-transduction in the presence of the indicated compound concentrations. Error bars are the standard error of the mean (SEM); ***$P < 0.001$; **$P < 0.01$; n.s. = not significant from an unpaired Student's t-test with unequal variance. In panel C, the FRET response was completely lost within the 1 to 50 nM change, therefore, an actual dose response could not be observed. (D, F) Firefly luciferase assay readouts from dose response series using the indicated compounds. Vectors were normalized on RT activity before transduction. Relative light units (RLU) were normalized for protein content of the transduced cell lysates and are displayed relative to the DMSO control. Shown is the average of a representative experiment performed in triplicate. Error bars indicate the standard deviation on triplicate data points.

DISCUSSION

It is generally accepted that the enzymatic function and quaternary structure of retroviral INs are closely intertwined. However, the molecular details about the spatiotemporal regulation of IN stoichiometry during the early steps of replication, prior to integration, remain largely unknown. An in-depth understanding of the stoichiometry and interaction with host factors driving alterations in the quaternary structure provides new structural and mechanis-

tic insights in the integration process which in the case of MLV could lead towards safer viral vectors for gene therapy. In this work, we employed single-virus fluorescence microscopy to provide insights in the MLV IN oligomeric state during early MLV replication. We present evidence that IN, the main component of the MLV PIC together with the viral genome derived vDNA, forms stable oligomeric complexes until completion of mitosis and that the BET proteins (Brd2-4), that has previously been shown to be a gammaretroviral integration cofactor (11–13), alters the quaternary IN structure when the PIC is tethered to the post-mitotic chromatin.

A fully functional fluorescent version of MLV for studying pre-integration steps

We generated fluorescently labeled MLV vectors carrying a fluorescent protein (mTurquoise2, mVenus or eGFP) directly fused to IN (41,60) (Figure 1A). We first corroborated that the MLV IN-FP modified MLV particles display wild-type processing (Figure 1B, Supplementary Figure S2A and transduction efficiency (Figure 1C,D). and the fluorescent MLV PICs closely follow the host cell cycle, as mitosis is required for granting PIC access to the nucleus (1,43) (Figure 4E). We corroborated this here; when blocked at the G1/S border by aphidicolin treatment, a much lower percentage of cells contained nuclear viral complexes (Figure 4E). The few cells that did contain nuclear complexes, possibly were already in mitosis when treated with aphidicolin or, alternatively, the viral complexes in these cells entered the nucleus by dead-end pathways. Supporting the notion of non-functional nuclear complexes, Roe *et al*. detected >100-fold less MLV integration events in aphidicolin-arrested cells (43).

By imaging the viruses early post-infection, we showed that IN-FP colocalized with CA early after transduction (Figure 4C, D). During mitosis the viral complexes were tethered to the metaphase DNA (Figure 4C) (5,9) through the action of p12 (Figure 5B). Finally, a time-dependent reduction in the number of cells with nuclear PIC complexes was observed (Figure 4D), an effect that we could ascribe, at least in part, to integration-dependent PIC dissociation since transduction in the presence of RAL partly prevented this drop (Figure 3G).

Taken together, we clearly showed that fluorescent labeling of MLV particles, by direct fusion of IN with a fluorescent protein, is a valid and powerful strategy for visualizing the early steps in the MLV replication cycle, with a defined focus on the IN enzyme.

Chromosome-mediated PIC retention by MLV versus active nucleopore filtering by HIV

Retroviruses developed various strategies to access the host chromatin. HIV PICs, with a size of ∼100 nm (61–63), require a significant reduction in size prior to nuclear entry to pass through the nuclear pore complex, which normally only allows passive passage of macromolecules up to ∼39 nm (64). In contrast to HIV, gammaretroviruses such as MLV only gain access to the chromosomes during mitosis, upon nuclear envelope breakdown. Association of p12 with mitotic chromosomes is crucial for retaining PICs in the nucleus after mitosis, as we've clearly corroborated (Figure 5B) (1,2,43). Interestingly, and in contrast to our previous observations for HIV, no reduction in the IN-FP content of nuclear MLV PICs was observed (Figure 4A and B). This result therefore indirectly supports our molecular filter hypothesis, that states that only HIV-1 PICs with a reduced IN content can enter the nucleus via the nucleopore (40).

Differential interaction with IN of MLV and HIV co-factors

Using a similar FRET approach we recently showed that LEDGF/p75, the HIV-1 tethering counterpart of BET proteins, induces a specific alteration in the HIV-1 IN oligomer in the nucleus (40). As expected, LEDGF/p75 had no influence on the MLV IN oligomer (Supplementary Figure S4). On the contrary, in the post-mitotic nucleus the MLV-IN oligomer underwent specific changes in the quaternary structure evidenced by an increased FRET signal (Figure 4E), because of interactions of the PIC with BET proteins (Figure 5E). It is known that HIV and MLV markedly differ in their interaction with their cognate cellular binding partners (17,65–68). While the LEDGF/p75 binding pocket is conserved among different lentiviral integrases, the corresponding fragments in other retroviral INs exhibit significant differences (65). In the LEDGF/p75 binding pocket of IN, a short interhelical loop of the IN binding domain (IBD) docks into a narrow V shaped cavity formed at the interface of a dimer of IN CCD molecules (65,69). These essential interacting features of LEDGF/p75 and HIV-1 IN are absent in the interface between BET proteins and MLV IN. For BET proteins, recent reports clarified the role of the additional unique 28 amino acid C-terminal (Ct) tail of MLV IN that directly binds the ET domain of BET proteins (11,17,18). This Ct is largely disordered, but undergoes a disorder-to-order transition upon complex formation with the ET domain, generating complementary pairing of charged and hydrophobic residues on both molecules (17,70). Interestingly, ectopic expression of the LEDGF/p75 IBD can inhibit HIV-1 integration (71–73), and the mere IBD binding changes the quaternary structure of HIV IN PICs (40). Overexpression of the ET of BET proteins, on the other hand stimulates MLV integration (12) and is unlikely to deregulate the IN catalytic function. Although it is tempting to conclude that BET proteins directly increase IN oligomerization, structural evidence suggests that other interactions, such as binding to DNA, are likely assisting in this process.

BET proteins ready the intasome for integration

The viral protein p12 is composed of two major domains. The N-terminal domain has been shown to stabilize the mature MLV core through a direct interaction with CA, thus preventing a premature loss of CA (6,7). Stabilization of the capsid core occurs through binding of the p12 N-terminus to the C-terminus. Disruption of this interaction by phosphorylation of the S61 position in p12 by a cell cycle kinase is critical to destabilize the capsid core and for regulating capsid uncoating, revealing the p12 chromatin tethering motif (C-terminus) to bind the PIC to the host chromatin

for nuclear retention after mitosis (8). The C-terminus of p12 is known to escort and tether the MLV PIC to mitotic chromosomes. Through this mechanism, p12 retains the PIC within the nucleus after the reformation of the nuclear envelope at the end of mitosis, which is required for subsequent integration (5,9,10). Introduction of the PM14 mutation in the p12 region of the MLV genome indeed interfered with chromatin tethering of the MLV PIC (Figure 5B) (5,9) and transduction (Figure 5C). Contrary to this, chromatin tethering mediated by p12 has been shown to have no direct influence on integration target site selection (10).

Preceding p12 chromosome tethering, CA dissociates from the PIC in mitotic cells, as we and other clearly showed ((9) and Figure 4C). No overlap between IN-FP and CA was observed in the post-mitotic nucleus (Figure 4C). These results corroborate findings that lower ratios of overlap were observed between CA and IN in PICs extracted from nuclear fractions compared to the cytoplasmic fractions, and that thus already suggested that CA is lost from the PIC after nuclear entry (74). Importantly, this capsid dissociation has been suggested before to expose the complex to interactions with cellular cofactors necessary for targeted integration (9).

The BET proteins (Brd2, Brd3 and Brd4) were recently identified to tether the MLV PIC to the host chromatin by directly interacting with IN (11–13,17,18). Furthermore, BET proteins are known to act as chromatin readers, targeting the PIC to transcription start sites and stimulating integration (11–13,17). Here we showed that Brd4 co-immunoprecipitated with IN-FP, but not with the BET interaction deficient mutant, IN(W390A)-FP, corroborating that Brd4 can indeed interact with the labeled IN (Figure 5D). Next, we showed that only upon exit from mitosis a BET protein-mediated alteration in the quaternary structure of the MLV IN oligomer occurs, which is abolished by the W390A substitution (Figure 5E) (57). Meanwhile, however, the PIC IN content remained constant (Figure 5F) and the oligomerization properties of the mutant IN are not affected (Supplementary Figures S5 and S6). Importantly, the FRET signal depended on the interactions of BET proteins with the PIC (Figure 5E) and the chromatin (Figure 6B–D) in the nucleus of post-mitotic cells. Contrary to this, IN catalytic activity was not required for the FRET signal (Figure 4F). The dose dependent inhibition by RAL and JQ1(+) of nuclear FRET increase correlated significantly with the inhibition of MLV transduction, as evidenced by a Spearman rank coefficient of 0.87 for the RAL data and 0.71 for the JQ1(+) data. Apparently, interference with BET-induced alterations in the quaternary structure of MLV IN, aborts infection underlining its importance. Interestingly, MLV carrying W390A IN, replicates without BET-induced IN alteration, suggesting an alternative integration mechanism. Here, we provide evidence using FRET that BET proteins induce an alteration in the quaternary structure change of IN as part of an integration-readying process of the host chromatin bound MLV pre-integration complex.

Based on our results, we propose a model (Figure 7) in which the MLV PIC, with a capsid core stabilized by p12 (6,7), is transported from the cytoplasm to the mitotic chromosomes without changes in IN content (constant fluorescence intensity) or quaternary structure (constant FRET signal). Before binding to the mitotic chromosomes, phosphorylation of p12 (S61) occurs, initiating CA uncoating and revealing the p12 chromosome tethering domain that attaches to the chromosomes during mitosis (7–9). MLV PIC tethering throughout mitosis does not affect the IN content of the viral complexes and is unrelated to CA-uncoating. In the nucleus of post-mitotic interphase cells the IN complex is exposed to nuclear proteins such as BET proteins (11–13,17,18). BET proteins target the nucleoprotein complex to the host chromatin thereby readying it for host genome integration. Binding of BET proteins requires a disorder-to-order transition of the C-terminal tail of the IN (21,70) which may affect the quaternary structure of the IN oligomer. This conformation presumably positions IN more favorably for effective integration at transcription start sites (TSS) and CpG islands. Future structural biology experiments using X-ray, protein NMR or smFRET

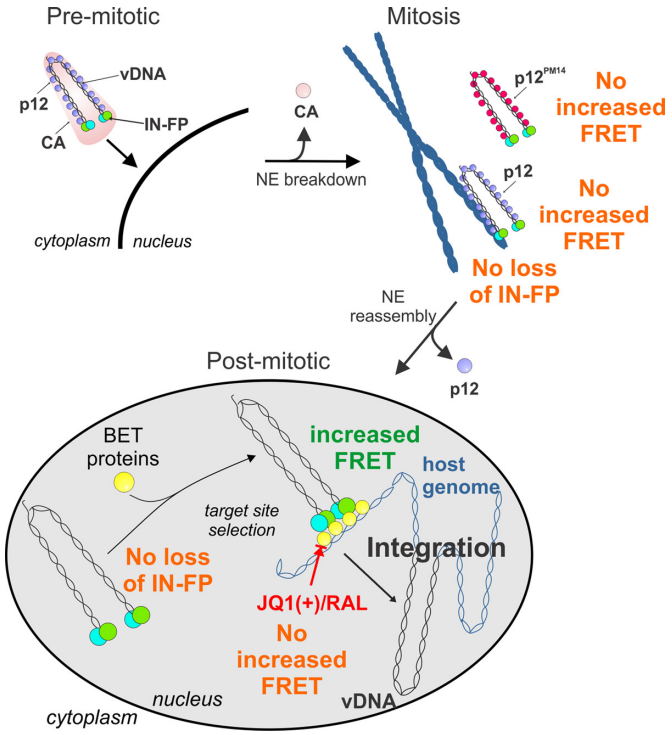

Figure 7. MLV pre-integration model. After entry in the cell, gradual uncoating events occur. The MLV PIC (with IN-FP proteins labeled by green and cyan circles), having a capsid core (light pink cone) stabilized by p12 (purple circles) (6,7), is transported to the mitotic chromosomes during mitosis. Upon phosphorylation of p12, the C-terminal domain is released, facilitating capsid uncoating and revealing the p12 chromatin tethering motif (7,8). After nuclear envelope breakdown, the MLV PIC (with IN-FP proteins labeled by green and cyan circles) is tethered via the C-terminus of the p12 viral protein (purple circles) to mitotic chromatin (blue) (5,9,10). Tethering of the p12 protein (purple circles) to mitotic chromosomes does not alter the IN content or quaternary structure. After nucleus reformation and release of p12, the IN complex is exposed to interactions with cellular cofactors, such as BET proteins (yellow circles) (11–13,17,18). In the nucleus of post-mitotic interphase cells, these BET proteins take over, tethering and targeting the nucleoprotein complex to the host DNA (blue), thereby readying it for host genome integration by inducing essential quaternary structural changes, such as alterations in stoichiometry and/or conformational rearrangements. Interference of this interaction using a W390A IN mutant or the BET-protein (JQ1(+)) or IN (RAL) inhibitors prevents this structural alteration.

on purified intasome components may provide conclusive evidence. Interference with chromatin reading or integrase strand transfer precludes the conformational change, indicating the formation of a ternary complex between BET, MLV IN and chromatin.

We have previously shown that BET-independent MLV viruses replicate with similar titers as WT virus in cell culture (56). Still, BET-independent MLV integration is clearly retargeted to a more random distribution away from transcriptional start sites (56). This difference in integration preference is apparently not phenocopied in viral replication in cell culture. Although strictly spoken the observed BET-mediated alteration in IN quaternary structure is thus not required for MLV replication in cell culture, authentic MLV virus and vector integration is mediated by BET and thus associated with the observed alteration in quaternary structure. The observed FRET increase may therefore reflect formation of an optimally targeted MLV IN complex. Recent evidence shows that Brd4 is a histone acetyl transferase that evicts nucleosomes from chromatin, thereby increasing chromatin accessibility (75). This activity may link Brd4 with optimal integration targeting and integration itself. This mechanism could explain the timing of the FRET increase to a post-mitotic event. Mouse experiments are ongoing to reveal a potential requirement of BET-mediated integration *in vivo*. Interestingly, the observed FRET increase does phenocopy the previously reported LEDGF/p75-mediated FRET increase of the HIV intasome in the nucleus (40), implying a general underlying mechanism.

In conclusion, we believe this work has increased the understanding of MLV integration, highlighting for the first time a BET-dependent change in the quaternary structure of the intasome in the nucleus of post-mitotic cells. This change may correspond to a conformational switch or to an increase in the affinity of the multimer. This study provides a platform to address further mechanistic questions related to MLV intasome dynamics.

SUPPLEMENTARY DATA

Supplementary Data are available at NAR Online.

ACKNOWLEDGEMENTS

Prof. Johan Hofkens is thanked for providing access to his fluorescence imaging facilities and critically reading the manuscript. The phCMV-intron Gag-Pol was a kind gift from François-Loic Cosset, LVRTG, ENS de Lyon–U412 121 INSERM, Lyon, France. We thank Dr Christine Kozak and Esther Shaffer (NIH/NIAID, Bethesda, MD) for the anti-RT antibody. We are grateful to Paulien Van de Velde, Nam Joo Van der Veken, Maarten Vervecken, Robbert Boudewijns and Els de Ridder for technical assistance. We thank Dr Jan de Rijck (KU Leuven) for critically reading the manuscript. D.B. acknowledges the agency for Innovation by Science and Technology (IWT Flanders). A.A., L.D., F.D.W. acknowledge the Research Foundation Flanders (FWO Vlaanderen) for their doctoral scholarships.

Author contributions: Conceptualization, D.B., J.He., Z.D.; methodology, D.B., I.Z., L.D., A.C.; software, L.D., J.He; investigation, D.B., I.Z., F.D.W., A.A, L.D., J.He., Z.D.; writing – original draft, D.B., J.He., Z.D.; Writing – Review & Editing, D.B., L.D., J.He., Z.D.; funding acquisition, J.He, Z.D.; resources: Z.D.; supervision, J.He., Z.D.

FUNDING

FWO [G0B49.15]; KU Leuven Research Council [OT; OT/13/098]; HIV-ERA EURECA [IWT-SBO-EURECA]; KU Leuven IDO program [IDO/12/008]; Belgian IAP Belvir and the Methusalem program [CASAS METH/08/04]. Funding for open access charge: project finance.

Conflict of interest statement. None declared.

REFERENCES

1. Suzuki,Y. and Craigie,R. (2007) The road to chromatin - nuclear entry of retroviruses. *Nat. Rev. Microbiol.*, **5**, 187–196.
2. Lewis,P.F. and Emerman,M. (1994) Passage through mitosis is required for oncoretroviruses but not for the human immunodeficiency virus. *J. Virol.*, **68**, 510–516.
3. Cohen,S., Au,S. and Pante,N. (2011) How viruses access the nucleus. *Biochim. Biophys. Acta*, **1813**, 1634–1645.
4. Bowerman,B., Brown,P.O., Bishop,J.M. and Varmus,H.E. (1989) A nucleoprotein complex mediates the integration of retroviral DNA. *Genes Dev.*, **3**, 469–478.
5. Prizan-Ravid,A., Elis,E., Laham-Karam,N., Selig,S., Ehrlich,M. and Bacharach,E. (2010) The Gag cleavage product, p12, is a functional constituent of the murine leukemia virus pre-integration complex. *PLoS Pathog.*, **6**, e1001183.
6. Wight,D.J., Boucherit,V.C., Nader,M., Allen,D.J., Taylor,I.A. and Bishop,K.N. (2012) The gammaretroviral p12 protein has multiple domains that function during the early stages of replication. *Retrovirology*, **9**, 83.
7. Wight,D.J., Boucherit,V.C., Wanaguru,M., Elis,E., Hirst,E.M., Li,W., Ehrlich,M., Bacharach,E. and Bishop,K.N. (2014) The N-terminus of murine leukaemia virus p12 protein is required for mature core stability. *PLoS Pathog.*, **10**, e1004474.
8. Brzezinski,J.D., Felkner,R., Modi,A., Liu,M. and Roth,M.J. (2016) Phosphorylation requirement of murine leukemia virus p12. *J. Virol.*, **90**, 11208–11219.
9. Elis,E., Ehrlich,M., Prizan-Ravid,A., Laham-Karam,N. and Bacharach,E. (2012) p12 tethers the murine leukemia virus pre-integration complex to mitotic chromosomes. *PLoS Pathog.*, **8**, e1003103.
10. Schneider,W.M., Brzezinski,J.D., Aiyer,S., Malani,N., Gyuricza,M., Bushman,F.D. and Roth,M.J. (2013) Viral DNA tethering domains complement replication-defective mutations in the p12 protein of MuLV Gag. *Proc. Natl. Acad. Sci. U.S.A.*, **110**, 9487–9492.
11. De Rijck,J., de Kogel,C., Demeulemeester,J., Vets,S., El Ashkar,S., Malani,N., Bushman,F.D., Landuyt,B., Husson,S.J., Busschots,K. *et al.* (2013) The BET family of proteins targets moloney murine leukemia virus integration near transcription start sites. *Cell Rep.*, **5**, 886–894.
12. Gupta,S.S., Maetzig,T., Maertens,G.N., Sharif,A., Rothe,M., Weidner-Glunde,M., Galla,M., Schambach,A., Cherepanov,P. and Schulz,T.F. (2013) Bromo- and extraterminal domain chromatin regulators serve as cofactors for murine leukemia virus integration. *J. Virol.*, **87**, 12721–12736.
13. Sharma,A., Larue,R.C., Plumb,M.R., Malani,N., Male,F., Slaughter,A., Kessl,J.J., Shkriabai,N., Coward,E., Aiyer,S.S. *et al.* (2013) BET proteins promote efficient murine leukemia virus integration at transcription start sites. *Proc. Natl. Acad. Sci. U.S.A.*, **110**, 12036–12041.
14. Mitchell,R.S., Beitzel,B.F., Schroder,A.R., Shinn,P., Chen,H., Berry,C.C., Ecker,J.R. and Bushman,F.D. (2004) Retroviral DNA integration: ASLV, HIV, and MLV show distinct target site preferences. *PLoS Biol.*, **2**, E234.

15. Wu,X., Li,Y., Crise,B. and Burgess,S.M. (2003) Transcription start regions in the human genome are favored targets for MLV integration. *Science*, **300**, 1749–1751.
16. LeRoy,G., Chepelev,I., DiMaggio,P.A., Blanco,M.A., Zee,B.M., Zhao,K. and Garcia,B.A. (2012) Proteogenomic characterization and mapping of nucleosomes decoded by Brd and HP1 proteins. *Genome Biol.*, **13**, R68.
17. Aiyer,S., Swapna,G.V., Malani,N., Aramini,J.M., Schneider,W.M., Plumb,M.R., Ghanem,M., Larue,R.C., Sharma,A., Studamire,B. *et al.* (2014) Altering murine leukemia virus integration through disruption of the integrase and BET protein family interaction. *Nucleic Acids Res.*, **42**, 5917–5928.
18. Larue,R.C., Plumb,M.R., Crowe,B.L., Shkriabai,N., Sharma,A., DiFiore,J., Malani,N., Aiyer,S.S., Roth,M.J., Bushman,F.D. *et al.* (2014) Bimodal high-affinity association of Brd4 with murine leukemia virus integrase and mononucleosomes. *Nucleic Acids Res.*, **42**, 4868–4881.
19. Cherepanov,P., Maertens,G.N. and Hare,S. (2011) Structural insights into the retroviral DNA integration apparatus. *Curr. Opin. Struct. Biol.*, **21**, 249–256.
20. Lewinski,M.K. and Bushman,F.D. (2005) Retroviral DNA integration–mechanism and consequences. *Adv. Genet.*, **55**, 147–181.
21. Aiyer,S., Rossi,P., Malani,N., Schneider,W.M., Chandar,A., Bushman,F.D., Montelione,G.T. and Roth,M.J. (2015) Structural and sequencing analysis of local target DNA recognition by MLV integrase. *Nucleic Acids Res.*, **43**, 5647–5663.
22. Jonsson,C.B., Donzella,G.A., Gaucan,E., Smith,C.M. and Roth,M.J. (1996) Functional domains of Moloney murine leukemia virus integrase defined by mutation and complementation analysis. *J. Virol.*, **70**, 4585–4597.
23. Yang,F., Leon,O., Greenfield,N.J. and Roth,M.J. (1999) Functional interactions of the HHCC domain of moloney murine leukemia virus integrase revealed by nonoverlapping complementation and zinc-dependent dimerization. *J. Virol.*, **73**, 1809–1817.
24. Guan,R., Aiyer,S., Cote,M.L., Xiao,R., Jiang,M., Acton,T.B., Roth,M.J. and Montelione,G.T. (2017) X-ray crystal structure of the N-terminal region of Moloney murine leukemia virus integrase and its implications for viral DNA recognition. *Proteins*, **85**, 647–656.
25. Studamire,B. and Goff,S.P. (2008) Host proteins interacting with the Moloney murine leukemia virus integrase: multiple transcriptional regulators and chromatin binding factors. *Retrovirology*, **5**, 48.
26. Engelman,A., Bushman,F.D. and Craigie,R. (1993) Identification of discrete functional domains of HIV-1 integrase and their organization within an active multimeric complex. *EMBO J.*, **12**, 3269–3275.
27. Guiot,E., Carayon,K., Delelis,O., Simon,F., Tauc,P., Zubin,E., Gottikh,M., Mouscadet,J.F., Brochon,J.C. and Deprez,E. (2006) Relationship between the oligomeric status of HIV-1 integrase on DNA and enzymatic activity. *J. Biol. Chem.*, **281**, 22707–22719.
28. Faure,A., Calmels,C., Desjobert,C., Castroviejo,M., Caumont-Sarcos,A., Tarrago-Litvak,L., Litvak,S. and Parissi,V. (2005) HIV-1 integrase crosslinked oligomers are active in vitro. *Nucleic Acids Res.*, **33**, 977–986.
29. Li,M., Mizuuchi,M., Burke,T.R. Jr and Craigie,R. (2006) Retroviral DNA integration: reaction pathway and critical intermediates. *EMBO J.*, **25**, 1295–1304.
30. Maertens,G.N., Hare,S. and Cherepanov,P. (2010) The mechanism of retroviral integration from X-ray structures of its key intermediates. *Nature*, **468**, 326–329.
31. Hare,S., Maertens,G.N. and Cherepanov,P. (2012) 3′-processing and strand transfer catalysed by retroviral integrase in crystallo. *EMBO J.*, **31**, 3020–3028.
32. Ballandras-Colas,A., Brown,M., Cook,N.J., Dewdney,T.G., Demeler,B., Cherepanov,P., Lyumkis,D. and Engelman,A.N. (2016) Cryo-EM reveals a novel octameric integrase structure for betaretroviral intasome function. *Nature*, **530**, 358–361.
33. Yin,Z., Shi,K., Banerjee,S., Pandey,K.K., Bera,S., Grandgenett,D.P. and Aihara,H. (2016) Crystal structure of the Rous sarcoma virus intasome. *Nature*, **530**, 362–366.
34. Passos,D.O., Li,M., Yang,R., Rebensburg,S.V., Ghirlando,R., Jeon,Y., Shkriabai,N., Kvaratskhelia,M., Craigie,R. and Lyumkis,D. (2017) Cryo-EM structures and atomic model of the HIV-1 strand transfer complex intasome. *Science*, **355**, 89–92.
35. Ballandras-Colas,A., Maskell,D.P., Serrao,E., Locke,J., Swuec,P., Jonsson,S.R., Kotecha,A., Cook,N.J., Pye,V.E., Taylor,I.A. *et al.* (2017) A supramolecular assembly mediates lentiviral DNA integration. *Science*, **355**, 93–95.
36. Jones,K.S., Coleman,J., Merkel,G.W., Laue,T.M. and Skalka,A.M. (1992) Retroviral integrase functions as a multimer and can turn over catalytically. *J. Biol. Chem.*, **267**, 16037–16040.
37. Jonsson,C.B. and Roth,M.J. (1993) Role of the His-Cys finger of Moloney murine leukemia virus integrase protein in integration and disintegration. *J. Virol.*, **67**, 5562–5571.
38. Villanueva,R.A., Jonsson,C.B., Jones,J., Georgiadis,M.M. and Roth,M.J. (2003) Differential multimerization of Moloney murine leukemia virus integrase purified under nondenaturing conditions. *Virology*, **316**, 146–160.
39. Yeager,M., Wilson-Kubalek,E.M., Weiner,S.G., Brown,P.O. and Rein,A. (1998) Supramolecular organization of immature and mature murine leukemia virus revealed by electron cryo-microscopy: implications for retroviral assembly mechanisms. *Proc. Natl. Acad. Sci. U.S.A.*, **95**, 7299–7304.
40. Borrenberghs,D., Dirix,L., De Wit,F., Rocha,S., Blokken,J., De Houwer,S., Gijsbers,R., Christ,F., Hofkens,J., Hendrix,J. *et al.* (2016) Dynamic oligomerization of integrase orchestrates HIV nuclear entry. *Sci. Rep.*, **6**, 36485.
41. Quercioli,V., Di Primio,C., Casini,A., Mulder,L.C., Vranckx,L.S., Borrenberghs,D., Gijsbers,R., Debyser,Z. and Cereseto,A. (2016) Comparative analysis of HIV-1 and murine leukemia virus three-dimensional nuclear distributions. *J. Virol.*, **90**, 5205–5209.
42. Yuan,B., Li,X. and Goff,S.P. (1999) Mutations altering the moloney murine leukemia virus p12 Gag protein affect virion production and early events of the virus life cycle. *EMBO J.*, **18**, 4700–4710.
43. Roe,T., Reynolds,T.C., Yu,G. and Brown,P.O. (1993) Integration of murine leukemia virus DNA depends on mitosis. *EMBO J.*, **12**, 2099–2108.
44. Pizzato,M., Erlwein,O., Bonsall,D., Kaye,S., Muir,D. and McClure,M.O. (2009) A one-step SYBR Green I-based product-enhanced reverse transcriptase assay for the quantitation of retroviruses in cell culture supernatants. *J. Virol. Methods*, **156**, 1–7.
45. Filippakopoulos,P., Qi,J., Picaud,S., Shen,Y., Smith,W.B., Fedorov,O., Morse,E.M., Keates,T., Hickman,T.T., Felletar,I. *et al.* (2010) Selective inhibition of BET bromodomains. *Nature*, **468**, 1067–1073.
46. Dedecker,P., Duwe,S., Neely,R.K. and Zhang,J. (2012) Localizer: fast, accurate, open-source, and modular software package for superresolution microscopy. *J. Biomed. Opt.*, **17**, 126008.
47. Roth,M.J., Tanese,N. and Goff,S.P. (1985) Purification and characterization of murine retroviral reverse transcriptase expressed in Escherichia coli. *J. Biol. Chem.*, **260**, 9326–9335.
48. Bao,K.K., Wang,H., Miller,J.K., Erie,D.A., Skalka,A.M. and Wong,I. (2003) Functional oligomeric state of avian sarcoma virus integrase. *J. Biol. Chem.*, **278**, 1323–1327.
49. Deprez,E., Tauc,P., Leh,H., Mouscadet,J.F., Auclair,C. and Brochon,J.C. (2000) Oligomeric states of the HIV-1 integrase as measured by time-resolved fluorescence anisotropy. *Biochemistry*, **39**, 9275–9284.
50. van den Ent,F.M., Vos,A. and Plasterk,R.H. (1999) Dissecting the role of the N-terminal domain of human immunodeficiency virus integrase by trans-complementation analysis. *J. Virol.*, **73**, 3176–3183.
51. Fletcher,T.M. 3rd, Soares,M.A., McPhearson,S., Hui,H., Wiskerchen,M., Muesing,M.A., Shaw,G.M., Leavitt,A.D., Boeke,J.D. and Hahn,B.H. (1997) Complementation of integrase function in HIV-1 virions. *EMBO J.*, **16**, 5123–5138.
52. Petit,C., Schwartz,O. and Mammano,F. (1999) Oligomerization within virions and subcellular localization of human immunodeficiency virus type 1 integrase. *J. Virol.*, **73**, 5079–5088.
53. Borrenberghs,D., Thys,W., Rocha,S., Demeulemeester,J., Weydert,C., Dedecker,P., Hofkens,J., Debyser,Z. and Hendrix,J. (2014) HIV virions as nanoscopic test tubes for probing oligomerization of the integrase enzyme. *ACS Nano*, **8**, 3531–3545.
54. Steinrigl,A., Nosek,D., Ertl,R., Gunzburg,W.H., Salmons,B. and Klein,D. (2007) Mutations in the catalytic core or the C-terminus of murine leukemia virus (MLV) integrase disrupt virion infectivity and exert diverse effects on reverse transcription. *Virology*, **362**, 50–59.
55. Debyser,Z., Christ,F., De Rijck,J. and Gijsbers,R. (2015) Host factors for retroviral integration site selection. *Trends Biochem. Sci.*, **40**, 108–116.

56. El Ashkar,S., Van Looveren,D., Schenk,F., Vranckx,L.S., Demeulemeester,J., De Rijck,J., Debyser,Z., Modlich,U. and Gijsbers,R. (2017) Engineering Next-Generation BET-Independent MLV vectors for safer gene therapy. *Mol. Ther. Nucleic Acids*, **7**, 231–245.
57. El Ashkar,S., De Rijck,J., Demeulemeester,J., Vets,S., Madlala,P., Cermakova,K., Debyser,Z. and Gijsbers,R. (2014) BET-independent MLV-based vectors target away from promoters and regulatory elements. *Mol. Ther. Nucleic Acids*, **3**, e179.
58. Kanno,T., Kanno,Y., Siegel,R.M., Jang,M.K., Lenardo,M.J. and Ozato,K. (2004) Selective recognition of acetylated histones by bromodomain proteins visualized in living cells. *Mol. Cell*, **13**, 33–43.
59. Espeseth,A.S., Felock,P., Wolfe,A., Witmer,M., Grobler,J., Anthony,N., Egbertson,M., Melamed,J.Y., Young,S., Hamill,T. *et al.* (2000) HIV-1 integrase inhibitors that compete with the target DNA substrate define a unique strand transfer conformation for integrase. *Proc. Natl. Acad. Sci. U.S.A.*, **97**, 11244–11249.
60. Voelkel,C., Galla,M., Maetzig,T., Warlich,E., Kuehle,J., Zychlinski,D., Bode,J., Cantz,T., Schambach,A. and Baum,C. (2010) Protein transduction from retroviral Gag precursors. *Proc. Natl. Acad. Sci. U.S.A.*, **107**, 7805–7810.
61. Lelek,M., Di Nunzio,F., Henriques,R., Charneau,P., Arhel,N. and Zimmer,C. (2012) Superresolution imaging of HIV in infected cells with FlAsH-PALM. *Proc. Natl. Acad. Sci. U.S.A.*, **109**, 8564–8569.
62. Briggs,J.A., Wilk,T., Welker,R., Krausslich,H.G. and Fuller,S.D. (2003) Structural organization of authentic, mature HIV-1 virions and cores. *EMBO J.*, **22**, 1707–1715.
63. Miller,M.D., Farnet,C.M. and Bushman,F.D. (1997) Human immunodeficiency virus type 1 preintegration complexes: studies of organization and composition. *J. Virol.*, **71**, 5382–5390.
64. Pante,N. and Kann,M. (2002) Nuclear pore complex is able to transport macromolecules with diameters of about 39 nm. *Mol. Biol. Cell*, **13**, 425–434.
65. Cherepanov,P., Ambrosio,A.L., Rahman,S., Ellenberger,T. and Engelman,A. (2005) Structural basis for the recognition between HIV-1 integrase and transcriptional coactivator p75. *Proc. Natl. Acad. Sci. U.S.A.*, **102**, 17308–17313.
66. Cherepanov,P. (2007) LEDGF/p75 interacts with divergent lentiviral integrases and modulates their enzymatic activity in vitro. *Nucleic Acids Res.*, **35**, 113–124.
67. Hare,S., Di Nunzio,F., Labeja,A., Wang,J., Engelman,A. and Cherepanov,P. (2009) Structural basis for functional tetramerization of lentiviral integrase. *PLoS Pathog.*, **5**, e1000515.
68. Hare,S., Shun,M.C., Gupta,S.S., Valkov,E., Engelman,A. and Cherepanov,P. (2009) A novel co-crystal structure affords the design of gain-of-function lentiviral integrase mutants in the presence of modified PSIP1/LEDGF/p75. *PLoS Pathog.*, **5**, e1000259.
69. Cherepanov,P., Sun,Z.Y., Rahman,S., Maertens,G., Wagner,G. and Engelman,A. (2005) Solution structure of the HIV-1 integrase-binding domain in LEDGF/p75. *Nat. Struct. Mol. Biol.*, **12**, 526–532.
70. Crowe,B.L., Larue,R.C., Yuan,C., Hess,S., Kvaratskhelia,M. and Foster,M.P. (2016) Structure of the Brd4 ET domain bound to a C-terminal motif from gamma-retroviral integrases reveals a conserved mechanism of interaction. *Proc. Natl. Acad. Sci. U.S.A.*, **113**, 2086–2091.
71. Meehan,A.M., Saenz,D.T., Morrison,J.H., Garcia-Rivera,J.A., Peretz,M., Llano,M. and Poeschla,E.M. (2009) LEDGF/p75 proteins with alternative chromatin tethers are functional HIV-1 cofactors. *PLoS Pathog.*, **5**, e1000522.
72. De Rijck,J., Vandekerckhove,L., Gijsbers,R., Hombrouck,A., Hendrix,J., Vercammen,J., Engelborghs,Y., Christ,F. and Debyser,Z. (2006) Overexpression of the lens epithelium-derived growth factor/p75 integrase binding domain inhibits human immunodeficiency virus replication. *J. Virol.*, **80**, 11498–11509.
73. Llano,M., Saenz,D.T., Meehan,A., Wongthida,P., Peretz,M., Walker,W.H., Teo,W. and Poeschla,E.M. (2006) An essential role for LEDGF/p75 in HIV integration. *Science*, **314**, 461–464.
74. Fassati,A. and Goff,S.P. (1999) Characterization of intracellular reverse transcription complexes of Moloney murine leukemia virus. *J Virol*, **73**, 8919–8925.
75. Devaiah,B.N., Case-Borden,C., Gegonne,A., Hsu,C.H., Chen,Q., Meerzaman,D., Dey,A., Ozato,K. and Singer,D.S. (2016) Brd4 is a histone acetyltransferase that evicts nucleosomes from chromatin. *Nat. Struct. Mol. Biol.*, **23**, 540–548.